Check for updates

JGR Atmospheres

RESEARCH ARTICLE
10.1029/2025JD045800

A 100-Year Record of Mineralogical Variations in Northeastern Greenland Ice-Core Dust: Insights From Individual Particle Analysis

N. Nagatsuka[1,2], K. Goto-Azuma[2], K. Nagashima[1], K. Fujita[3], Y. Komuro[2,4], M. Hirabayashi[2], J. Ogata[2], K. Fukuda[2], Y. Ogawa-Tsukagawa[2], K. Kitamura[2], A. Yonekura[5], F. Nakazawa[2], Y. Onuma[6], N. Kurita[7], S. O. Rasmussen[8], G. Sinnl[8,9], T. J. Popp[8], and D. Dahl-Jensen[8,10]

[1]Research Institute for Global Change, Japan Agency for Marine-Earth Science and Technology, Yokosuka, Japan, [2]National Institute of Polar Research, Tokyo, Japan, [3]Graduate School of Environmental Studies, Nagoya University, Nagoya, Japan, [4]Laboratory for Environmental Research at Mount Fuji, Tokyo, Japan, [5]Marine Works Japan Ltd., Yokosuka, Japan, [6]Meteorological Research Institute, Japan Meteorological Agency, Tsukuba, Japan, [7]Institute for Space-Earth Environmental Research, Nagoya University, Nagoya, Japan, [8]Physics of Ice, Climate, and Earth, Niels Bohr Institute, University of Copenhagen, Copenhagen, Denmark, [9]British Antarctic Survey, Cambridge, UK, [10]Centre for Earth Observation Science, University of Manitoba, Winnipeg, MB, Canada

Abstract Reconstructing mineral dust deposition on the Greenland Ice Sheet provides crucial insights into atmospheric circulation and climate variability. However, understanding spatial and temporal variations in Greenland ice-core mineral sources during the Holocene is challenging due to low dust concentrations. Here, we present the first continuous, high-temporal-resolution record of size, composition, and source variability of mineral dust from a northeastern Greenland ice core (EGRIP S3) covering 1910 to 2013 AD. Using a multi-proxy provenance approach based on individual particle analysis, we reconstruct temporal changes in ice-core dust sources. We apply recently developed provenance tracing techniques, namely scanning electron microscopy (SEM)-cathodoluminescence (CL) analysis of single quartz particles, and SEM energy-dispersive X-ray spectroscopy (EDS) analysis. The SEM-CL/EDS results indicate that the primary sources of EGRIP S3 ice-core dust are East Asian (Gobi and Taklimakan) and African (Sahara) deserts. Their relative contributions shifted since the 1960s–1970s, with Asian dust decreasing and African dust increasing, likely reflecting variations in the Atlantic Multidecadal Oscillation and the recent decline in Asian dust events. To investigate spatial variability in dust sources across Greenland, we compare the EGRIP S3 ice-core dust records with those from a northwestern coastal site (SIGMA-D). The comparison reveals distinct differences in variability and mineral composition, suggesting different geological sources. The SIGMA-D ice-core dust record reflects increased local dust input during warmer periods, whereas the EGRIP S3 ice-core dust shows low temporal variability, indicating a more stable, long-range dust supply with minimal local influence.

Plain Language Summary The history of mineral dust deposition on the Greenland Ice Sheet provides substantial insight into past climate and environmental changes. However, very little is known about the sources and variability of Greenland ice-core dust over the past several hundred years because the amount of dust is very small and difficult to analyze. To address this, we analyzed individual dust particles from a northeastern interior Greenland ice core, producing the first continuous, high-resolution record of dust particle size, composition, and sources covering 1910 to 2013 AD. The results reveal that the ice-core dust primarily originated from East Asian (Gobi and Taklimakan deserts) and African (Sahara Desert) deserts, with the contribution from Asian dust sources decreasing and African dust sources increasing since the 1960s–1970s. This shift is likely linked to cyclical variations in the sea surface temperature of the North Atlantic Ocean and the recent decline in Asian dust events. Comparison with a northwestern coastal Greenland ice core showed clear differences in dust variability and composition, reflecting local dust contribution and differences in geological sources. These findings indicate that the sources and transport of mineral dust differ between the interior and coastal regions of Greenland.

Key Points:

- A 100-year high-temporal-resolution record of mineral composition and sources was reconstructed from a northeastern Greenland ice core
- The primary mineral sources are Asian and African deserts, with relative contributions shifting since the 1960s–1970s
- This shift is likely linked to variations in the Atlantic Multidecadal Oscillation and reduced Asian dust events

Supporting Information:

Supporting Information may be found in the online version of this article.

Correspondence to:

N. Nagatsuka,
nagatsukan@jamstec.go.jp

Citation:

Nagatsuka, N., Goto-Azuma, K., Nagashima, K., Fujita, K., Komuro, Y., Hirabayashi, M., et al. (2026). A 100-year record of mineralogical variations in northeastern Greenland ice-core dust: Insights from individual particle analysis. *Journal of Geophysical Research: Atmospheres*, *131*, e2025JD045800. https://doi.org/10.1029/2025JD045800

Received 20 NOV 2025
Accepted 15 OCT 2026

Author Contributions:

Conceptualization: N. Nagatsuka
Data curation: N. Nagatsuka, K. Goto-Azuma, K. Nagashima, K. Fujita, Y. Komuro, M. Hirabayashi, J. Ogata, K. Fukuda, Y. Ogawa-Tsukagawa, K. Kitamura, A. Yonekura, F. Nakazawa, N. Kurita, S. O. Rasmussen, G. Sinnl
Formal analysis: N. Nagatsuka, K. Nagashima, K. Fujita, Y. Komuro, F. Nakazawa

© 2026 The Author(s). Journal of Geophysical Research: Atmospheres published by Wiley Periodicals LLC on behalf of American Geophysical Union. This is an open access article under the terms of the Creative Commons Attribution License, which permits use, distribution and reproduction in any medium, provided the original work is properly cited.

Funding acquisition: N. Nagatsuka, K. Goto-Azuma, Y. Komuro, M. Hirabayashi, F. Nakazawa, Y. Onuma, D. Dahl-Jensen
Investigation: N. Nagatsuka, K. Goto-Azuma, K. Nagashima, K. Fujita, Y. Komuro, M. Hirabayashi, J. Ogata, K. Fukuda, Y. Ogawa-Tsukagawa, K. Kitamura, A. Yonekura, F. Nakazawa, Y. Onuma, N. Kurita, S. O. Rasmussen, G. Sinnl, T. J. Popp, D. Dahl-Jensen
Methodology: N. Nagatsuka, K. Nagashima
Project administration: K. Goto-Azuma, D. Dahl-Jensen
Resources: K. Goto-Azuma, K. Nagashima, M. Hirabayashi
Software: Y. Onuma
Visualization: N. Nagatsuka, K. Fujita, Y. Komuro, Y. Onuma
Writing – original draft: N. Nagatsuka, K. Nagashima, K. Fujita, Y. Komuro, Y. Onuma, N. Kurita
Writing – review & editing: K. Goto-Azuma, K. Nagashima, K. Fujita

1. Introduction

The history of dust deposition on the Greenland Ice Sheet reconstructed from ice cores provides substantial insight into past climate and environmental changes. Ice-core mineral dust exhibits significant variations in concentration, particle size, and composition over different time scales (e.g., Schüpbach et al., 2018; Steffensen, 1997; Whitlow et al., 1992). For example, on glacial-interglacial timescales (e.g., from the Eemian to the Holocene), ice-core dust records show a strong correlation with climate variability, as indicated by $\delta^{18}O$ records. Dust concentrations in central Greenland ice cores increased by a factor of 100 during the Last Glacial Maximum compared to those in the Holocene and show a strong correlation with temperature (Fuhrer et al., 1999; Schüpbach et al., 2018; Steffensen, 1997). On seasonal timescales, dust from a northwestern Greenland firn ice core (NEEM, Gfeller et al., 2014) as well as that from snow on the northwest (NEEM, Kuramoto et al., 2011), northeast (EGRIP, Nakazawa et al., 2021; Komuro et al., 2024), central (Summit, Drab et al., 2002; Whitlow et al., 1992), and south Greenland Ice Sheet (SE-Dome, Oyabu et al., 2016) show seasonality characterized by a peak concentration in springtime during the Holocene. For the North Greenland Ice Core Project (NGRIP) ice core, the present-day dust concentration varies from >140 μg kg^{-1} in the spring to >20 μg kg^{-1} in the autumn (Bory, Biscaye, & Grousset, 2003). Glacial-interglacial shifts and seasonal variability in dust deposition may be related to the effects of climate change, environmental changes in dust sources such as their extent and aridity, and changes in atmospheric transport (Svensson et al., 2000).

Greenland ice-core dust not only provides valuable information for paleoclimate and paleoenvironmental reconstruction but also influences the mass balance of the ice sheet, as well as atmospheric processes in the Arctic. Recently, areas of "dark ice" have appeared and expanded on the ice-sheet surface (Shimada et al., 2016), which are thought to contribute to the recent reduction in surface albedo and increased melting rates of the Greenland Ice Sheet (e.g., Alexander et al., 2014; Shimada et al., 2016; Wientjes et al., 2011). One likely cause of this darkening is the increased accumulation of cryoconite, a mixture and/or aggregate of mineral dust and organic matter produced by microbial activity on glacier surfaces (e.g., Chandler et al., 2015; Takeuchi et al., 2014). Mineral dust is the principal constituent of cryoconite and provides nutrients that promote microbial growth, thereby contributing to its accumulation. In particular, englacial dust that had been deposited from the atmosphere in the upstream regions, traveled through the ice sheet, and outcropped again in the ablation zone has been found to play a key role in cryoconite formation in ablation zones (Nagatsuka et al., 2016). This dust was likely deposited widely on the ice sheet in the past and thus preserved in ice cores. Differences in dust mineralogy likely influence nutrient availability for glacier microorganisms, thereby affecting microbial abundance and community composition on glacier surfaces (Nagatsuka et al., 2018). These microorganisms are major constituents of cryoconite and play a central role in its formation and development (Cook et al., 2016; Hodson et al., 2010). Thus, reconstructing variations in the composition and sources of ice-core minerals that are expected to be exposed on the ice surface in the future is essential for evaluating the impact of dust on upcoming darkening events as well as on the magnitude of ice mass loss of the Greenland Ice Sheet. In addition to its role in surface processes, the physical and chemical characteristics of mineral dust, such as particle size and composition, also affect atmospheric processes, as certain minerals act as effective ice-nucleating particles that influence cloud formation and radiative forcing in the Arctic (e.g., Atkinson et al., 2013; DeMott & Prenni, 2010; Murray et al., 2012). Since the efficiency of mineral dust as ice-nucleating particles strongly depends on mineral type, crystal structure, and surface properties (e.g., Atkinson et al., 2013), characterizing the mineralogical composition of dust preserved in ice cores provides indirect constraints on past variability in ice-nucleating particle sources and potential properties. Furthermore, understanding how mineralogical composition and ice-nucleating particle characteristics vary under different climate states can help constrain projections of future changes in ice-nucleating particle activity. Therefore, to better understand the impact of mineral dust on the Greenland Ice Sheet and the climate system, it is essential to identify not only its provenance but also the size and composition of mineral dust particles archived in ice cores.

In Greenland ice-core studies, potential dust sources have predominantly been identified through geochemical analyses, particularly those based on strontium (Sr), neodymium (Nd), lead (Pb), uranium (U), and hafnium (Hf) isotope ratios. The isotope ratios for mineral dust in central Greenland ice cores, obtained by the Greenland Ice Sheet Project Two (GISP2) and the Greenland Ice Core Project (GRIP), suggest that the most probable sources of this dust are East Asian deserts and/or central European loess (Biscaye et al., 1997; Svensson et al., 2000; Újvári et al., 2015). Isotopic analyses of the Dye-3 ice core also suggest contributions from East Asian deserts, with additional mixing from Saharan dust (Lupker et al., 2010). North Africa is also considered as a potential source

21698996, 2026, 22, Downloaded from https://agupubs.onlinelibrary.wiley.com/doi/10.1029/2025JD045800 by NICE, National Institute for Health and Care Excellence, Wiley Online Library on [19/11/2026]. See the Terms and Conditions (https://onlinelibrary.wiley.com/terms-and-conditions) on Wiley Online Library for rules of use; OA articles are governed by the applicable Creative Commons License

21698996, 2026, 22, Downloaded from https://agupubs.onlinelibrary.wiley.com/doi/10.1029/2025JD045800 by NICE, National Institute for Health and Care Excellence, Wiley Online Library on [19/11/2026]. See the Terms and Conditions (https://onlinelibrary.wiley.com/terms-and-conditions) on Wiley Online Library for rules of use; OA articles are governed by the applicable Creative Commons License

(Újvári et al., 2022). On the other hand, the isotope ratios for minerals found in an ice core obtained from southeastern coastal Greenland indicate that the dust originated from local sources (Simonsen et al., 2019). However, these radiogenic isotope analyses generally require sub-mg to mg-scale amounts of dust (e.g., Svensson et al., 2000; Újvári et al., 2022) and thus primarily target ice-core dust originating from glacial periods characterized by high dust concentration. For the NGRIP ice core, Ruth et al. (2003) found the highest dust concentrations (4–8 mg dust/kg ice) in stadial periods and relatively low concentrations (0.3–0.7 mg dust/kg ice) in interstadial periods. Several studies have attempted to measure the isotope ratios (e.g., Sr, Nd, Pb, U, and Hf) in Greenlandic ice-core dust from the Holocene (e.g., 8.2–11.6 ka: Han et al., 2018, 4–7 ka: Simonsen et al., 2019, over several decades in the 1600s: Bory, Biscaye, Piotrowski, & Steffensen, 2003, over several years in the 1700s: Lupker et al., 2010), a period characterized by much lower dust concentration (less than 0.1 mg dust/kg ice in interior Greenland ice cores; Vallelonga & Svensson, 2014) than that in a glacial period. Under such low-dust conditions (i.e., during the Holocene), a single sample with radiogenic Sr, Nd, Pb, U, and Hf data thus requires the averaging of ice over tens to hundreds of years. Therefore, there is little high-temporal-resolution data on the sources and variability of mineral dust over the last several hundred years, a period increasingly affected by human activities, including land-use change and rising anthropogenic greenhouse gas concentrations. These changes may contribute to aridification in some regions, potentially affecting dust emissions (e.g., Huang et al., 2017; Webb & Pierre, 2018). To tackle this problem, alternative approaches based on individual particle analyses have been developed. Nagatsuka et al. (2021) analyzed the morphology and mineralogy of individual dust particles in a northwestern Greenland ice core using scanning electron microscopy (SEM) and energy-dispersive X-ray spectroscopy (EDS). SEM provides morphological information, while EDS provides the elemental composition of individual particles, allowing the identification of mineral assemblages characteristic of different source regions and thus enabling provenance assessment even under low dust concentrations. In terms of analytical efficiency, radiogenic isotope analyses require relatively large amounts of sample material and several days of sample preparation, whereas isotopic measurements themselves are largely automated and relatively rapid (1 hr/sample) once the samples are prepared. On the other hand, SEM-based individual particle analyses require relatively simple sample preparation but involve more labor-intensive manual particle identification and characterization (several days/sample). Although SEM-based approaches provide less definitive provenance constraints compared with isotope-based methods, they can be applied to samples with very low dust concentrations and enable reconstruction of temporal variations at much higher temporal resolution. Nagatsuka et al. (2021) produced historical records of mineral dust sources for the past 100 years with a resolution of 5 years, thus demonstrating the effectiveness of this approach for determining variations in the sources of ice-core mineral dust during periods of low dust concentration. Furthermore, Nagashima et al. (2026) utilized SEM–cathodoluminescence (CL) analysis of individual quartz particles to elucidate seasonal variations in dust provenance within a Canadian ice core, demonstrating that Asian dust is predominant during most seasons whereas Saharan dust becomes dominant in winter. These results highlight the utility of individual-particle SEM-based approaches as a complementary tool to isotope-based methods, particularly for reconstructing high-resolution dust source variability under low-dust conditions.

Ice-core dust sources probably vary geographically even within the Greenland Ice Sheet because environmental conditions, such as altitude and distance from the coast, differ greatly among regions (e.g., Bory, Biscaye, Piotrowski, & Steffensen, 2003; Kjær et al., 2022). The interior of the ice sheet generally has the highest elevation (Bamber et al., 2013; Helm et al., 2014). Bory, Biscaye, Piotrowski, and Steffensen (2003) analyzed samples from the 11th and 17th–18th centuries and reported that the dust transported over long distances was deposited at almost all elevated interior sites on the ice sheet, whereas it was likely that the dust from local ground sources was present only at coastal sites. This distinction seems to depend on the distance from the ice sheet margin and/or altitude (Bory, Biscaye, Piotrowski, & Steffensen, 2003). Furthermore, atmospheric transport may also affect the geographical variations in mineral dust sources over the ice sheet. Based on the compositional variations of ice-core minerals and a back-trajectory analysis, it has been reported that the air mass and dust at the northwestern ice sheet (SIGMA-D site) originated from the west coast of Greenland and northern Canada during the period 1950–2004 AD (Nagatsuka et al., 2021). On the other hand, the air mass and dust at the central ice sheet (GISP2, GRIP, and NGRIP sites) likely originated mostly from Asia, Europe, and North Africa during the period 45–12 ka BP as well as the 17th century (Bory, Biscaye, Piotrowski, & Steffensen, 2003; Svensson et al., 2000; Újvári et al., 2015, 2022). The primary source of dust in southeastern Greenland (Dye-3 site) was estimated to be Asia, with North Africa as an additional source in the 18th century (Lupker et al., 2010). Although differences in geographical conditions may have led to nonuniform dust deposition over the ice sheet, spatial variations in the continuous records for the Greenland ice-core dust sources have still not been clarified. Since the SIGMA-D site

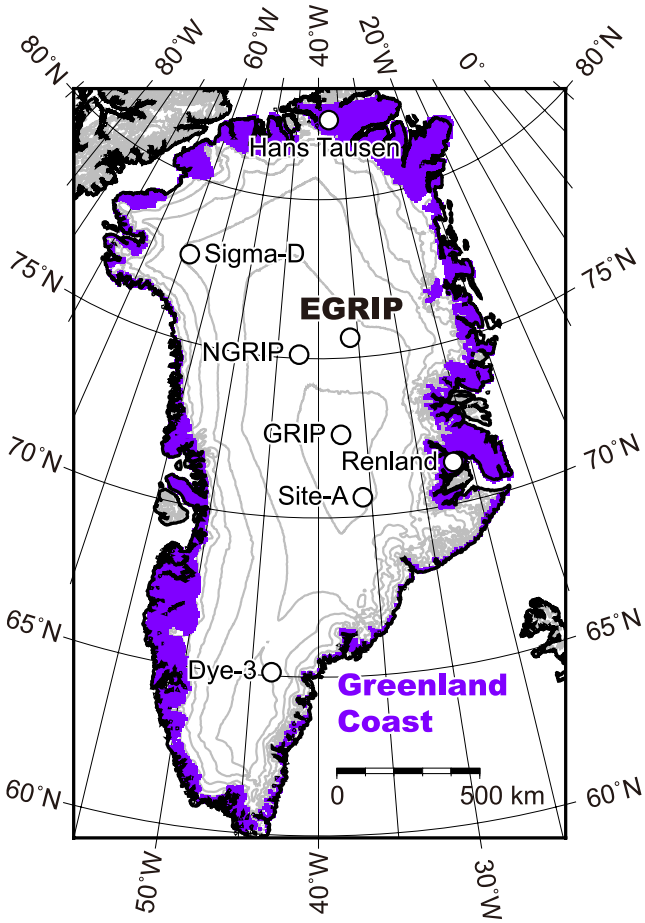


Figure 1. Location map of the EGRIP ice-core site (75.38°N, 36.00°W, 2,708 m above sea level), where the EGRIP S3 shallow ice core was drilled, and SIGMA-D, Hans Tausen, NGRIP, GRIP, Renland, Site-A, and Dye-3 ice-core sites used for back-trajectory comparison. Contour lines are drawn at 500-m intervals. The purple shaded region denotes the ice-free coastal terrain (GrC).

is located relatively close to the margin of the ice sheet, local dust contributions are significant, making it difficult to identify dust from distant sources (Nagatsuka et al., 2021). Therefore, identifying dust sources in ice cores from more interior sites with high temporal resolution should provide new insights into long-range dust transport to Greenland and its temporal variability.

This paper describes the temporal and geographical variations in ice-core dust sources from the interior of the Greenland Ice Sheet. We present the first continuous records of the size and composition, as well as the temporal variations in potential sources, of mineral dust preserved in an ice core obtained from the northeastern Greenland Ice Sheet spanning from 1910–2013 AD. The East Greenland Ice Core Project (EGRIP), which is an international ice coring project spearheaded by the University of Copenhagen, Denmark, was launched in 2015 as the first deep ice coring project in the northeastern interior ice sheet (Goto-Azuma et al., 2021). In this study, the size and mineral composition of individual dust particles in a shallow ice core from the EGRIP site (EGRIP S3 ice core) are analyzed using SEM and EDS. Additionally, we apply the recently developed provenance tracing approach based on SEM-CL analysis of individual quartz particles (Nagashima et al., 2017, 2023, 2026) to the EGRIP S3 ice core to improve the precision of ice-core dust source identification during periods of low dust concentration. SEM-CL detects intrinsic defects and impurities in quartz that vary depending on conditions during its formation and subsequent geological history (Zinkernagel, 1978). This enables the characterization of dust sources based on differences of bedrock types (volcanic, plutonic, and metamorphic rocks), which exhibit distinct CL spectra (Götte & Richter, 2006; Götze et al., 2001, 2021; Zinkernagel, 1978), using only a small amount of sample. However, some overlap in CL spectral characteristics among different bedrock types has been reported (e.g., Boggs et al., 2002; Zinkernagel, 1978), which limits the ability to uniquely determine bedrock types from individual quartz particles. Despite this limitation, CL spectra remain a useful tool for provenance studies, particularly when used to identify relative contributions from different source regions. The results are compared to data from the northwestern coastal Greenland ice core (SIGMA-D), as analyzed by Nagatsuka et al. (2021), to identify regional variations in dust sources within the ice sheet.

2. Samples and Analytical Methods

2.1. EGRIP S3 Ice Core

The ice core was drilled at an elevation of 2,708 m above sea level, approximately 1.2 km south of the EGRIP deep drilling site (75.38°N, 36.00°W) in July 2017 (Figure 1). The EGRIP site is located 470 km inland from the eastern coast of Greenland and close to the onset of the Northeast Greenland Ice Stream, which is the largest ice stream on the Greenland Ice Sheet (Joughin et al., 2010; Vallelonga et al., 2014). The ice core was recovered from a depth of 1.51–133.09 m.

2.2. Analyses of Major Elements, Microparticles, and Tritium in EGRIP S3 Ice Core

To date the EGRIP S3 ice core, the sodium (Na), sulfate (SO_4), and tritium concentrations were measured. Na concentrations were used for annual layer counting based on their seasonal variability, whereas sulfate concentrations were used to identify volcanic marker horizons. Tritium concentrations were used to identify the tritium peak derived from atmospheric nuclear weapons testing, which serves as an additional chronological marker horizon. Na and S concentrations were continuously measured below a depth of 1.51 m. Tritium concentrations were measured using ice-core samples collected at 0.04-m intervals between depths of 13–15 m. Detailed analytical procedures are described in Appendix A.

21698996, 2026, 22, Downloaded from https://agupubs.onlinelibrary.wiley.com/doi/10.1029/2025JD045800 by NICE, National Institute for Health and Care Excellence, Wiley Online Library on [19/11/2026]. See the Terms and Conditions (https://onlinelibrary.wiley.com/terms-and-conditions) on Wiley Online Library for rules of use; OA articles are governed by the applicable Creative Commons License

21698996, 2026, 22, Downloaded from https://agupubs.onlinelibrary.wiley.com/doi/10.1029/2025JD045800 by NICE, National Institute for Health and Care Excellence, Wiley Online Library on [19/11/2026]. See the Terms and Conditions (https://onlinelibrary.wiley.com/terms-and-conditions) on Wiley Online Library for rules of use; OA articles are governed by the applicable Creative Commons License

For comparison with the mineral composition determined using SEM-EDS, we measured the concentrations of elements that originated from terrestrial dust using the same inductively coupled plasma mass spectrometry (ICP-MS) system as that used for Na and SO_4 measurements (Goto-Azuma et al., 2024, 2025). These elements included silicon (Si), aluminum (Al), magnesium (Mg), potassium (K), calcium (Ca), and iron (Fe). Silicon, Al, and Fe predominantly originated from terrestrial dust, and some of the Mg, K, and Ca originated from sea salt. Under the assumption that Na solely originated from sea salt, we calculated the non-sea-salt (nss) fractions, which mainly originated from terrestrial dust, as follows:

$$[\mathrm{nssCa}] = [\mathrm{Ca}] - (\mathrm{Ca/Na})_{\mathrm{sea}} \times [\mathrm{Na}], \quad (1)$$

where $(\mathrm{Ca/Na})_{\mathrm{sea}}$ is the mass ratio of Ca to Na in seawater, which is 0.037 (Savarino & Legrand, 1998). Similarly, the concentrations of nssMg and nssK were calculated using the mass ratio of Mg to Na (0.12) and that of K to Na (0.037) in seawater, respectively (Savarino & Legrand, 1998). On average, the nss fractions of Ca, Mg, and K accounted for 96%, 67%, and 88% of the total concentrations of these elements, respectively.

For dust particle size and concentration measurements, a portion of the meltwater was collected from the continuous-flow analysis (CFA) samples taken at depth intervals of approximately 0.08 m w.e. using a fraction collector. The concentration of dust was measured by a Coulter counter (Multisizer 4e, Beckman Coulter, USA) using a 30-μm-aperture tube in a Class 10,000 clean room at the NIPR. The size bins covered the range of 0.7–18.0 μm.

2.3. SEM-EDS Analysis of Mineral Dust

To extract mineral dust from the ice core for SEM analysis, we first melted the ice-core samples and collected them in pre-cleaned glass vials in 10-year intervals. Next, a 500-μL aliquot from each well-mixed sample was filtered through a polycarbonate membrane filter (Advantec) with a diameter of 25 mm and a pore size of 0.1 μm in a Class 10,000 clean room. We determined the size and chemical composition of individual mineral dust particles using SEM (Quanta FEG 450, FEI) and EDS (X-Max 50, Oxford Instruments, UK) at the NIPR. The filter was attached to aluminum stubs using carbon tape and coated with a layer of platinum. Under the assumption of a uniform distribution of dust samples on the filter, we divided the filter into four equal sections and observed a total of 200 randomly selected particles from one of these sections. The equivalent circle diameter was measured using image-processing software (ImageJ, National Institutes of Health, USA). To minimize bias in the selection of mineral dust, particles were observed in various positions on one quarter of the filter over a span of a few days. Particle number size distributions and log-normal fitting results (fitting curves, mode diameters, and width parameters) were calculated using Igor Pro software (WaveMetrics, USA). The content levels of major elements and related oxides were determined from the EDS spectra. Details of the SEM-EDS analytical method are described in Nagatsuka et al. (2021).

2.4. Mineral Identification

Mineralogical identification of the EGRIP S3 ice-core dust was performed using three procedures (Nagatsuka et al., 2021): (a) matching of the spectral pattern for each particle to those for mineral standards (Severin, 2004); (b) comparison of the morphology and oxide composition of the ice-core dust to those of mineral standards; (c) application of the elemental peak intensity ratio sorting scheme used to identify Greenland ice-core (GISP2) mineral dust (Donarummo et al., 2003). The results of previous studies have demonstrated that a comparison of the results obtained using these procedures enables reliable identification of ice-core minerals (Maggi, 1997; Wu et al., 2016).

2.5. SEM-CL Analysis of Mineral Dust

To identify potential sources of the ice-core dust, we performed SEM-CL analysis on single quartz particles. First, we randomly selected 52–56 quartz particles from the EGRIP S3 ice core on each filter for six different periods (1940–1950, 1950–1960, 1970–1980, 1980–1990, 1990–2000, 2010–2013 AD) and analyzed them using SEM (Quanta FEG 450, FEI) and EDS (EDAX, Octane Elite 30) at the Japan Agency for Marine-Earth Science and Technology (JAMSTEC). Then, we measured their CL spectrum from 350 to 830 nm at 3.3-nm intervals using SEM combined with a CL system (Gatan, Mono CL4 Swift) at JAMSTEC. The settings were the same as those

21698996, 2026, 22, Downloaded from https://agupubs.onlinelibrary.wiley.com/doi/10.1029/2025JD045800 by NICE, National Institute for Health and Care Excellence, Wiley Online Library on [19/11/2026]. See the Terms and Conditions (https://onlinelibrary.wiley.com/terms-and-conditions) on Wiley Online Library for rules of use; OA articles are governed by the applicable Creative Commons License

reported by Nagashima et al. (2023, 2026), with the measurement time ranging from 2 to 5 s per particle depending on the CL emission intensity of each particle. The measured CL spectra were then corrected for the instrument's total response using the response correction curve supplied by Gatan Inc. and are presented in energy units (eV).

As a reference for North America, a potential dust source region, we also analyzed 38 quartz particles in a surface dust (cryoconite) sample collected from a mountain glacier in Alaska (Gulkana Glacier, 63°14′N, 145°42′W, Figure S1 in Supporting Information S1). This sample was previously analyzed for Sr-Nd isotope ratios and is denoted as S5 in Nagatsuka et al. (2018). The isotopic values were similar to those of Alaskan loess, indicating that the sample is dominated by locally derived Alaskan sediments (Nagatsuka et al., 2018).

For quantitative evaluation, each CL spectrum converted in energy units was fitted with six Gaussian-shaped emission components (EC1–EC6), representing features linked to impurities or structural imperfections within the quartz (Nagashima et al., 2023). These components correspond to peaks at approximately 1.75, 1.9, 2.0, 2.2, 2.7, and between 2.9 and 3.2 eV, respectively (Table S1 in Supporting Information S1). The CL spectra of quartz particles, reflecting relative abundance of such emission components, varied with conditions during quartz crystallization, such as temperature and growth rate, as well as the metamorphic pressure-temperature conditions experienced afterward (e.g., Zinkernagel, 1978), resulting in characteristic patterns that vary with parent rock type, including volcanic, plutonic, or metamorphic rocks, with slight variations depending on the degree of metamorphism (e.g., Götte & Richter, 2006; Götze et al., 2001; Götze et al., 2021; Zinkernagel, 1978), although some overlap in these spectral characteristics has also been reported.

To quantify spectral features, Nagashima et al. (2023) performed a cluster analysis using Ward's method on the fractional areas of EC1–EC6 for quartz particles from East Asian deserts (the Gobi and Taklimakan deserts) and from seawater filtration samples collected in the Okhotsk and the Bering Seas. Quartz particles in the latter samples are primarily derived from the Amur and Yukon Rivers, whose drainage basins cover large areas of Siberia and Alaska. These quartz samples represented a wide range of terrestrial bedrocks. Their calculated cluster analysis dendrogram contained three clusters (Clusters 1–3), each defined by elevated abundances of EC1 and EC3, EC3 and EC6, and EC5 and EC6, respectively (Table S1 in Supporting Information S1). Based on previously reported relationships between the CL signatures of quartz and their source rock types (Boggs et al., 2002; Götte & Richter, 2006; Götze et al., 2001; Zinkernagel, 1978), Nagashima et al. (2023) inferred that Cluster 1 predominantly reflects quartz derived from low-grade metamorphic rocks or slowly cooled high-grade metamorphic rocks, whereas Clusters 2 and 3 correspond to quartz sourced from plutonic rocks and from volcanic or rapidly cooled high-grade metamorphic rocks, respectively. Although these clusters were originally derived from quartz particles collected across Asia, Siberia, and Alaska as described above, they reflect general CL signatures of three major rock types rather than region-specific characteristics.

Quartz particles in the EGRIP S3 filters and a surface dust sample from Alaska were classified into three clusters according to their CL spectra, following the method described in Nagashima et al. (2026). For each particle, we quantified the similarity to the cluster profiles (Table S1 in Supporting Information S1) by computing the sum of squared differences in the fractional areas of EC1–EC6, and assigned it to the closest cluster. The percentage contribution of Clusters 1–3 was subsequently calculated for each sample.

2.6. Back-Trajectory Analysis

The air mass transport pathways to the EGRIP site were analyzed using the Hybrid Single-Particle Lagrangian Integrated Trajectory (HYSPLIT) model (Stein et al., 2015). The initial air masses were set to 50, 500, 1000, and 1500 m above ground level at the EGRIP site for the 7-day back-trajectories. The probability distribution for the air mass within this altitude range (<1500 m above ground level) was calculated with 1° × 1° resolution. We assumed that the dust particles had been deposited via a wet process (Iizuka et al., 2018; Parvin et al., 2019), for which the probability was weighted by the daily precipitation on the date when the air mass arrived at the ice-core site (Nagatsuka et al., 2021). We used daily precipitation from the ERA5 reanalysis data set produced by the European Centre for Medium-Range Weather Forecasts (Hersbach et al., 2020). The regional contribution was also calculated from the probability distribution, for which land areas were divided into nine regions: the Greenland Ice Sheet (GrIS), the Greenland coast (GrC), North America (NA), Europe (EU), Russia (RUS), Central Asia (CA), Southeast Asia (SA), Middle East (ME), and Africa (AF) (Figure 2a). Considering the dust source, the ocean and GrIS were excluded from the calculation.

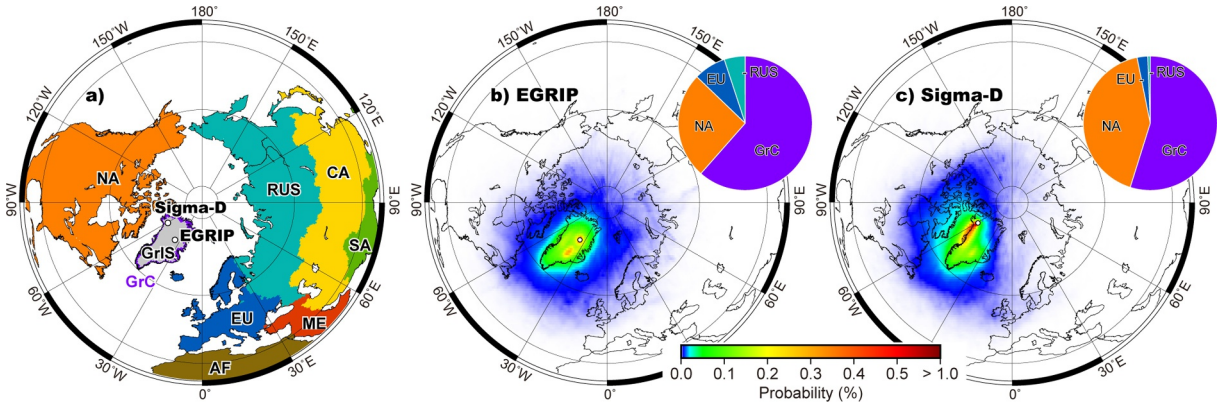


Figure 2. Maps showing (a) locations of EGRIP and SIGMA-D ice-core sites in Greenland, along with nine regions used to calculate regional contributions (GrIS: Greenland Ice Sheet, gray; GrC: Greenland coast, purple; NA: North America, orange; EU: Europe, blue; RUS: Russia, light blue; CA: Central Asia, yellow; SA: Southeast Asia, green; ME: Middle East, red; and AF: Africa, brown), and probability distribution for air mass at (b) EGRIP and (c) SIGMA-D sites from 7-day three-dimensional back-trajectory analysis from 1958 to 2014 AD. The probability distribution was calculated by summing the air mass trajectories at 50, 500, 1,000, and 1,500 m above ground level. The pie charts illustrate the cumulative source contribution over the 7-day back-trajectories from potential dust-source regions excluding the Greenland coastal region, calculated according to the regional definitions shown in panel (a). The total contribution from the included source regions is normalized to 100%, and the relative contributions of each region are presented. (a) and (c) are modified from Nagatsuka et al. (2021).

2.7. Snow Cover Fraction

To examine the surface conditions of adjacent source areas for mineral dust in the EGRIP S3 ice core, we analyzed inter-annual changes in snow cover fraction based on numerical climate model simulations. We used snow cover data derived from the land-historical experiment (1850–2014) in the Land Surface, Snow and Soil Moisture Model Intercomparison Project (LS3MIP; Hurk et al., 2016), part of the World Climate Research Program Coupled Model Intercomparison Project Phase 6 (CMIP6; Eyring et al., 2016). In this study, we examined the ensemble means of snow cover fraction simulated by 12 climate models, as listed in the Data Availability section. Anomalies in the summer (June–July–August) were calculated for the period 1915–2012, separately for northeastern and southeastern Greenland. These regions were divided at 70°N, following Nagatsuka et al. (2021).

3. Results

3.1. Dating of EGRIP S3 Ice Core

Ice-core dating was performed by counting annual layers of Na concentration, which showed clear seasonal variations (Figure A1). The observed seasonality of the water stable isotope ratios and chemical components in the ice cores and snowpack has been previously reported at various sites on the Greenland Ice Sheet and is often used for annual layer counting (Komuro et al., 2021; Kuramoto et al., 2011; Kurosaki et al., 2020; Legrand & Mayewski, 1997; Nagatsuka et al., 2021; Nakazawa et al., 2021; Oyabu et al., 2016; Sinnl et al., 2022; Whitlow et al., 1992). The winter season in the EGRIP S3 ice core was defined as the depth at which the Na concentration had a maximum value. The period from winter season to winter season was counted as 1 year.

Three fixed dates were provided by the ice layers, tritium profile, and SO_4 spikes. The ice layer at a depth of 2.14 m is assumed to correspond to summer 2012 AD based on a snow pit observation at EGRIP in summer 2017 (Komuro et al., 2021). We interpreted the ice layer at a depth of 2.40 m as a layer that formed via the refreezing of meltwater produced by surface melting in summer 2012 AD. The sharp tritium peak at a depth of 14.1 m corresponds to nuclear bomb testing in 1963 AD (Clausen & Hammer, 1988; Koide et al., 1982). The two sharp SO_4 peaks at depths of 23.17 and 23.30 m are presumed to be associated with the eruption of the Katmai volcano, Alaska, which occurred on June 6–8, 1912 AD (e.g., Hildreth, 1983; Hildreth & Fierstein, 2000; Sinnl et al., 2022). We assigned the latter peak to this eruption because this peak appears after the Na concentration peak (winter) and corresponds to the timing of the eruption in early summer. The SO_4 peak at a depth of 23.17 m, which is assumed to correspond to the 1913 AD winter/spring, is interpreted as stratospheric fallout of sulfate aerosols

21698996, 2026, 22, Downloaded from https://agupubs.onlinelibrary.wiley.com/doi/10.1029/2025JD045800 by NICE, National Institute for Health and Care Excellence, Wiley Online Library on [19/11/2026]. See the Terms and Conditions (https://onlinelibrary.wiley.com/terms-and-conditions) on Wiley Online Library for rules of use; OA articles are governed by the applicable Creative Commons License

21698996, 2026, 22, Downloaded from https://agupubs.onlinelibrary.wiley.com/doi/10.1029/2025JD045800 by NICE, National Institute for Health and Care Excellence, Wiley Online Library on [19/11/2026]. See the Terms and Conditions (https://onlinelibrary.wiley.com/terms-and-conditions) on Wiley Online Library for rules of use; OA articles are governed by the applicable Creative Commons License

produced by the same eruption, although it may also be derived from anthropogenic sulfate, peaking in winter to early spring (Beer et al., 1991; Kuramoto et al., 2011; Oyabu et al., 2016) and/or the eruption of the Hekla volcano, Iceland, starting on 24 April 1913 AD (Bigler et al., 2002). Volcanic aerosols from the 1912 Katmai eruption, the world's largest 20th-century volcanic eruption, were injected into the stratosphere and remained suspended until at least as late as December 1914 AD (e.g., Burke et al., 2019; Hildreth & Fierstein, 2012; Volz, 1975a, 1975b). Volcanic sulfate deposits from the stratosphere have also been found in the 1913 layer of other Arctic ice cores and are identified by a subsidiary SO_4 peak (Burke et al., 2019; Yalcin et al., 2007). From a comparison of the annual layer counts and these reference horizons, we estimated the ice-core dating uncertainty to be ±1 year. We also compared our EGRIP S3 chronology to the Greenland ice-core chronology 2021 (GICC21, Sinnl et al., 2022) based on multiple ice cores including the EGRIP main core. The two chronologies are in good agreement within their respective uncertainties. To confirm the ages in the bottom section of the analyzed ice-core sample, we also used the ice layers at depths of 27.32 and 27.33 m, which are assumed to correspond to summer 1889 AD. These layers have been identified in multiple ice cores from central Greenland (Alley & Koci, 1988; Clausen & Hammer, 1988; Meese et al., 1994) and northwest Greenland (Fischer et al., 1998). They are known to have formed via widespread surface melting events on the Greenland Ice Sheet in 1889 AD (Keegan et al., 2014).

From these analyses, we estimated that a depth of 23.64 m corresponds to the year 1910 AD and that the average accumulation rate for the period 1910–2013 AD was 0.11 m w.e. yr^{-1}. This rate is close to that for the period 1607–2011 at EGRIP reported by Vallelonga et al. (2014) (0.10 m w.e. yr^{-1}). Based on our chronology, the dates associated with the SO_4 peaks at 2.56, 9.20, and 23.17 m were estimated to be 2011, 1987, and 1913 AD, respectively. The existence of volcanic signals in these years is consistent with the results of previous ice-core studies at EGRIP (Kjær et al., 2016, 2022).

3.2. Particle Morphology

According to the number size distribution, the diameter of most particles was smaller than 2 μm (Table S2, Figures S2 and S3 in Supporting Information S1), similar to values reported for other Greenland ice cores (e.g., Biscaye et al., 1997; Nagatsuka et al., 2021; Steffensen, 1997). The mean particle diameter, calculated as 10-year-averaged values, ranged from 0.85 to 1.36 μm and the maximum particle diameter ranged from 5.06 to 8.94 μm. The size distribution varied depending on the period. The samples from 1910 to 1990 AD (except for samples from 1930 to 1940 and 1970 to 1980 AD) showed a slightly bimodal distribution with smaller peaks at 0.32–0.66 μm and larger peaks at 1.10–3.34 μm. On the other hand, the samples from 1990 to 2013 AD showed a unimodal distribution with peaks at 0.71–0.76 μm (Figure S3 in Supporting Information S1). No samples contained particles larger than 10 μm.

3.3. Quantitative Estimation of Dust Mineralogy

The EDS analysis showed that for all samples, the ice-core dust was composed predominantly of silicate minerals (86%–97%, Figures S4 and S5 in Supporting Information S1). The silicates were categorized as quartz, mafic minerals, Na/Ca-feldspar (plagioclase), K-feldspar (orthoclase/microcline), Na/K-feldspar (intermediate alkali feldspar), and clays, which included kaolinite, high-Si + Al minerals (possibly including kaolinite and pyrophyllite, see Text S1 in Supporting Information S1, for definition), smectite, illite, micas, and chlorite, along with mixed layers of illite/smectite and micas/chlorite (Figure 3 and Figure S4 in Supporting Information S1). We also observed a few particles with compositions similar to those of rhyolitic volcanic glass, which have been found in other Greenland ice cores (e.g., Cook et al., 2022). Based on the semi-quantitative EDS analysis, the proportion of the mica/chlorite mix was the highest (21%–37%) and that of smectite was the lowest (0%–2%) for all silicate mineral particles in nearly every period (Table 1, Figure 3). The proportions of high-Si + Al minerals, illite/smectite mix, illite, and quartz were the second highest, varying in the ranges 9%–22%, 4%–14%, 3%–16%, and 4%–12%, respectively.

The EGRIP S3 ice core exhibits relatively minor, but statistically significant differences in mineral composition across different age groups (a chi-square test on 11 age-defined samples [1910–2013 AD] and 13 mineral types, $p = 5.50 \times 10^{-10}$). Lower high-Si + Al mineral content and higher illite/smectite mix and illite content were found for the 1910–1970 samples (high-Si + Al minerals: 9%–14%, illite/smectite mix: 6%–14%, illite: 9%–16%) compared to those for the 1970–2013 samples (high-Si + Al minerals: 18%–22%, illite/smectite mix: 4%–5%, illite:

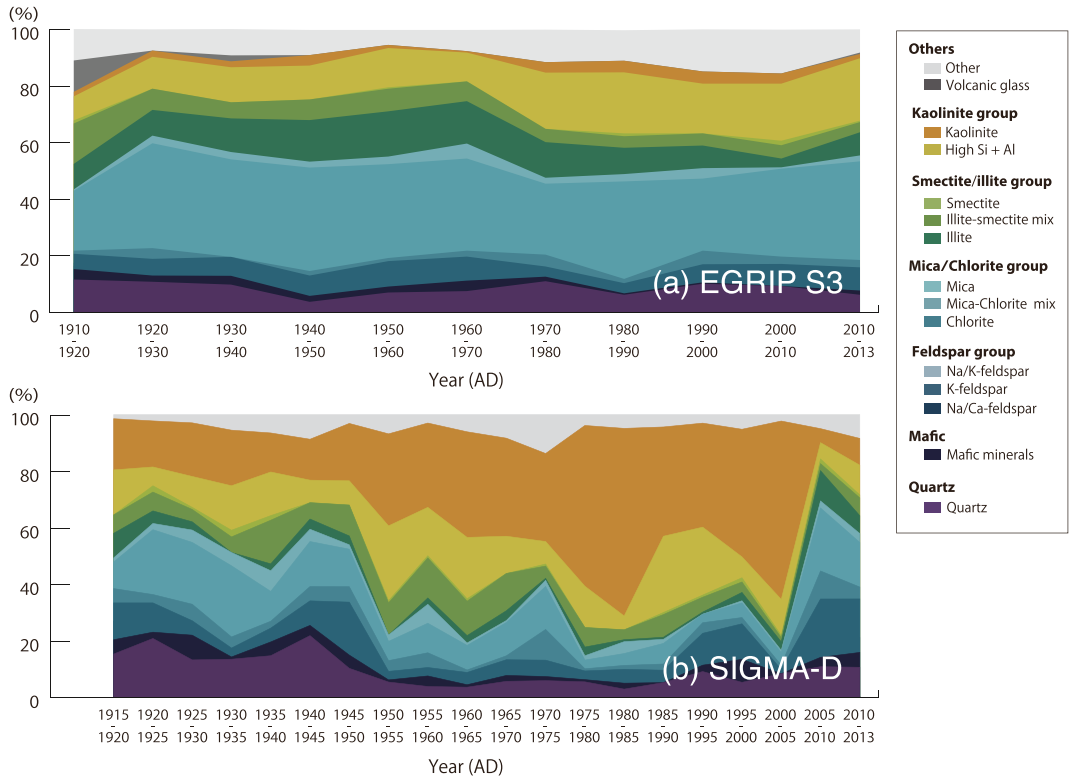


Figure 3. Variations of silicate mineral compositions in (a) the EGRIP S3 ice core (top) and (b) the SIGMA-D ice core (bottom) dust with 10- and 5-year resolutions, respectively. "Feldspar group" includes Na/K-feldspar, K-feldspar, and Na/Ca-feldspar.

3%–13%). A higher volcanic glass content (11%) was also found in the 1910–1920 sample compared to that in samples from other periods (0%–2%). The compositions of other silicate minerals were similar for the same periods.

The ice-core samples also contained non-silicate minerals, mainly Fe-dominant minerals, possibly including hematite, magnetite, or pyrite, at low concentrations (Figure S5 in Supporting Information S1). The relative abundance of these minerals was 2%–6% and showed low variation among the samples.

Table 1
Relative Abundance (%) of Silicate Mineral Groups for Each EGRIP S3 Sample

Sample	Kaolinite	High-Si + Al	Smectite	Illite/Smectite	Illite	Micas	Micas/Chlorite	Chlorite	Na/Ca-feldspar	K-feldspar	Na/K-feldspar	Mafic	Quartz	Volcanic glass	Unknown
1910–1920	1.6	8.5	1.1	14.3	9.0	0.5	21.2	1.1	3.2	1.1	1.1	3.7	11.6	11.1	11.1
1920–1930	2.2	11.3	0.0	7.5	9.1	2.7	37.1	3.8	4.3	1.6	0.0	2.2	10.8	0.0	7.5
1930–1940	2.1	12.4	0.0	5.7	11.9	2.6	34.5	0.0	5.2	1.0	0.5	3.1	9.8	2.1	9.3
1940–1950	3.7	12.0	0.0	7.3	14.7	2.1	36.6	1.6	3.1	3.1	1.0	2.1	3.7	0.0	8.9
1950–1960	1.1	13.9	0.5	8.0	16.0	2.7	33.2	1.1	8.0	0.5	0.5	2.1	7.0	0.0	5.3
1960–1970	0.5	10.2	0.0	7.0	15.0	5.3	32.6	2.1	4.3	2.1	2.1	3.7	7.5	0.0	7.5
1970–1980	3.7	19.9	0.0	4.7	12.6	2.1	25.1	4.2	2.6	0.0	1.0	1.6	11.0	0.0	11.5
1980–1990	4.1	21.6	1.0	4.1	9.3	2.6	34.5	1.5	2.6	1.0	0.0	0.5	6.2	0.0	10.8
1990–2000	4.3	17.6	0.0	4.3	8.0	3.7	25.5	4.8	4.8	1.6	0.0	0.5	10.1	0.0	14.9
2000–2010	3.6	20.2	1.6	4.7	3.1	0.5	31.1	2.6	6.2	0.0	1.6	0.0	9.3	0.0	15.5
2010–2013	1.5	22.1	0.5	3.6	8.2	2.1	34.9	2.6	5.1	2.6	0.5	1.5	6.2	0.5	8.2

21698996, 2026, 22, Downloaded from https://agupubs.onlinelibrary.wiley.com/doi/10.1029/2025JD045800 by NICE, National Institute for Health and Care Excellence, Wiley Online Library on [19/11/2026]. See the Terms and Conditions (https://onlinelibrary.wiley.com/terms-and-conditions) on Wiley Online Library for rules of use; OA articles are governed by the applicable Creative Commons License

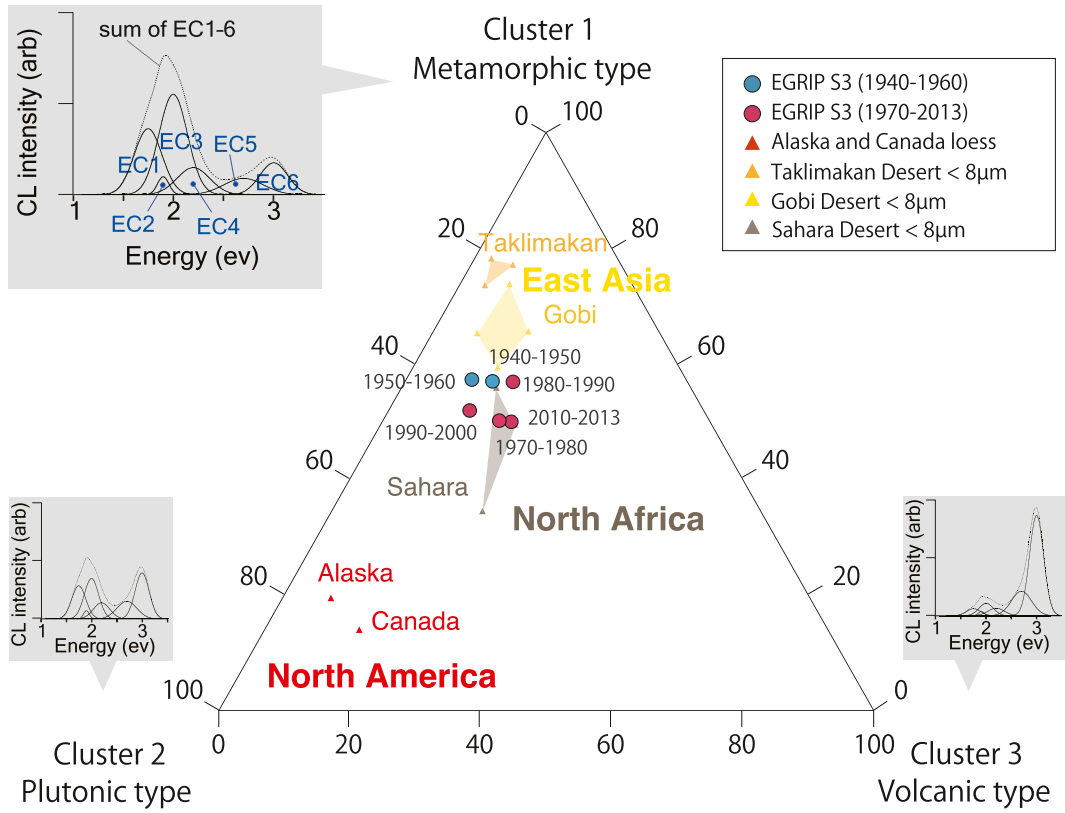


Figure 4. Cluster composition of quartz particles in the EGRIP S3 ice core from six periods (1940–1950, 1950–1960, 1970–1980, 1980–1990, 1990–2000, 2010–2013 AD) and those from Gobi Desert, Taklimakan Desert, and Sahara Desert (Nagashima et al., 2026) and North America (Alaska and Canada). Canadian data represent quartz particles (>8 μm) from the Mt. Logan ice core interpreted as locally derived dust (Nagashima et al., 2026). The relative abundances of the emission components (EC1–EC6) for each cluster are plotted near the corresponding corner points.

3.4. Cluster Compositions of Cathodoluminescence Spectra for Quartz Particles in EGRIP S3 Ice Core and Alaskan Cryoconite

The CL spectra of quartz particles in EGRIP S3 ice core and Alaskan cryoconite samples were successfully represented by six Gaussian-shaped emission components (EC1–EC6), and all particles could be assigned to one of the three clusters. The quartz particles in the EGRIP S3 ice-core samples from 1940 to 1950, 1950 to 1960, and 1980 to 1990 AD show a dominant contribution of Cluster 1 (57%–58%) with lesser contributions of Cluster 2 (27%–32%) and Cluster 3 (10%–16%) (Tables S3 and S4 in Supporting Information S1, Figure 4). On the other hand, the quartz particles in the samples from 1970 to 1980, 1990 to 2000, and 2010 to 2013 AD exhibit slightly lesser and higher contributions of Cluster 1 (50%–52%) and Cluster 2 (31%–36%), respectively, and a similar contribution of Cluster 3 (13%–19%) compared to those for the former three samples. Based on the cluster definitions provided in Section 2.5, the cluster compositions of the first three samples indicate a dominance of metamorphic-rock sources and fall between those of the Taklimakan, Gobi (Southern Mongolia), and Saharan deserts. The other three samples show a rather larger contribution from plutonic rocks, which is similar to the cluster composition of the Sahara Desert.

In contrast, quartz particles in the supraglacial cryoconite samples from Alaska show a dominant contribution of Cluster 2 (73%), with relatively minor contributions from Clusters 1 (20%) and 3 (7%), a pattern clearly distinct from that observed in the EGRIP S3 samples (Tables S3 and S4 in Supporting Information S1, Figure 4).

21698996, 2026, 22, Downloaded from https://agupubs.onlinelibrary.wiley.com/doi/10.1029/2025JD045800 by NICE, National Institute for Health and Care Excellence, Wiley Online Library on [19/11/2026]. See the Terms and Conditions (https://onlinelibrary.wiley.com/terms-and-conditions) on Wiley Online Library for rules of use; OA articles are governed by the applicable Creative Commons License

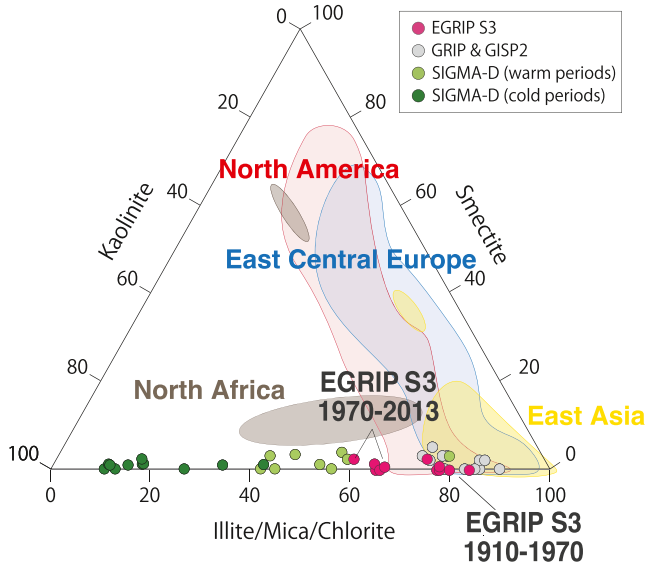


Figure 5. Ternary clay mineralogy diagram of EGRIP S3 ice-core dust from 1910 to 2013, plotted together with published data for Greenland Ice Sheet Project 2 (GISP2) and Greenland Ice Core Project (GRIP) ice-core dust from the Last Glacial Maximum (Biscaye et al., 1997; Svensson et al., 2000), modern SIGMA-D ice-core dust (Nagatsuka et al., 2021), and potential source areas (PSAs) in illite/micas/chlorite-smectite-kaolinite space. Colored envelopes represent the compositional ranges defined by the individual data sets. The "kaolinite" category for EGRIP S3 dust includes both kaolinite and high-Si + Al minerals (see Text S1 in Supporting Information S1, for definition).

4. Discussion

4.1. Potential Sources of EGRIP S3 Ice-Core Minerals

The EGRIP S3 ice-core dust samples from 1910 to 2013 AD primarily consisted of silicate minerals (Figure S5 in Supporting Information S1), the most common mineral group in Earth's crust (Deer et al., 1993), including quartz, feldspars, clay minerals (illite, chlorite, mica, smectite, and kaolinite), and minor mafic minerals. The silicate mineral compositions in the EGRIP S3 ice core have notably low variations among the samples (Figure 3), indicating that the sources remained relatively stable during this period.

To identify the ice-core dust sources, we applied SEM-CL analysis for the first time in Greenland ice-core dust provenance research. SEM-CL has allowed the characterization of quartz particles representing East Asian and African deserts and those from regional areas around Mount Logan, Canada (Nagashima et al., 2023, 2026). The quartz particles in the EGRIP S3 ice core exhibit cluster compositions closely resembling those of East Asian deserts (Gobi and Taklimakan deserts) and the Sahara Desert (Figure 4), suggesting that these East Asian and African deserts are likely the primary sources of the ice-core dust. This finding aligns with previous results for other interior Greenland ice-core dust during glacial periods (e.g., Biscaye et al., 1997; Han et al., 2018; Svensson et al., 2000; Újvári et al., 2022) based on Sr, Nd, Pb, U, and Hf isotope ratios.

The interpretation of the primary sources of the ice-core dust is further supported by both particle size and mineral composition. The ice-core dust is predominantly composed of fine particles smaller than 2 μm (Figures S2 and S3 in Supporting Information S1), indicative of long-range atmospheric transport (e.g., Simonsen et al., 2019). Further compositional evidence is provided by a ternary clay mineralogy diagram, which shows the proportions of illite/micas/chlorite, kaolinite, and smectite (Figure 5). This diagram reveals that the EGRIP S3 ice-core dust samples are similar to loess from East Asia, especially from the Taklimakan and Gobi deserts and the central Loess Plateau (Figure S6 in Supporting Information S1), as well as to dust from other interior Greenland ice cores (GRIP, Svensson et al., 2000; GISP2, Maggi, 1997). The EGRIP S3 ice core also shows a similar kaolinite proportion but slightly lower smectite proportion compared to those of the Sahara Desert (Figure S6 in Supporting Information S1). This difference can be explained by smectite fractionation during atmospheric transport (Scheuvens et al., 2013; Singer et al., 2004). The Sahara Desert thus remains a plausible dust source.

Although the mineralogical evidence consistently indicates that East Asian and African deserts are the primary dust sources, the HYSPLIT back-trajectory analysis suggests only negligible air-mass contributions from these regions (Figure 2b). This discrepancy likely reflects the limitations of back-trajectory analysis in representing long-range dust transport (Schüpbach et al., 2018), which tends to underestimate the contribution of distal dust sources. The back-trajectory analysis is therefore used only as supplementary evidence for evaluating the relative influence of nearby source regions. The provenance of distal dust discussed in this study is primarily interpreted based on the mineralogical and geochemical evidence obtained from the SEM-EDS and SEM-CL analyses.

Previous studies have suggested additional source regions for Greenland ice-core dust. Regional climate modeling by Újvári et al. (2022) indicated a plausible European dust contribution, which was transported into the Greenland interior after mixing with African dust. For EGRIP S3 ice-core dust samples from 1910 to 1970 AD, the values in a ternary clay mineralogy diagram are similar to those for a limited number of regions in Eastern Europe, such as Serbia and Ukraine (Figure S6 in Supporting Information S1). Although CL analyses were not performed for these samples and this interpretation therefore remains tentative, these regions are known as major loess source areas (e.g., Buggle et al., 2008; Jary & Ciszek, 2013) and may represent additional dust sources.

The ternary clay mineral diagram also shows overlaps between EGRIP S3 samples and loess deposits from several regions of North America including Yukon, Canada, and Alaska, Tennessee, Ohio, and Michigan, USA

21698996, 2026, 22, Downloaded from https://agupubs.onlinelibrary.wiley.com/doi/10.1029/2025JD045800 by NICE, National Institute for Health and Care Excellence, Wiley Online Library on [19/11/2026]. See the Terms and Conditions (https://onlinelibrary.wiley.com/terms-and-conditions) on Wiley Online Library for rules of use; OA articles are governed by the applicable Creative Commons License

21698996, 2026, 22, Downloaded from https://agupubs.onlinelibrary.wiley.com/doi/10.1029/2025JD045800 by NICE, National Institute for Health and Care Excellence, Wiley Online Library on [19/11/2026]. See the Terms and Conditions (https://onlinelibrary.wiley.com/terms-and-conditions) on Wiley Online Library for rules of use; OA articles are governed by the applicable Creative Commons License

(Figure S6 in Supporting Information S1). However, clay mineral ternary diagrams alone cannot clearly distinguish between geographically distinct dust sources. Our SEM-CL analyses indicate that Alaskan loess and Canadian loess differ significantly from the EGRIP S3 dust (Figure 4), suggesting that these two regions are unlikely to represent major dust sources. Ohio and Tennessee are extensive loess source regions (e.g., Muhs et al., 2001), which may contribute to long-range dust transport.

Nevertheless, previous provenance studies based on radiogenic isotope compositions generally indicate that the contribution of North America to Greenland ice-core dust is minor compared to those from East Asia and North Africa (e.g., Újvári et al., 2015, 2022). For example, Újvári et al. (2022) concluded that North America made only a minimal contribution to last glacial dust in central Greenland (GRIP and GISP2) based on Sr–Nd–Hf isotope analysis, even though some samples plot close to North American loess in clay mineral ternary diagrams (Figure 5, based on Újvári et al., 2022). Atmospheric transport modeling studies (Andersen et al., 1998; Mahowald et al., 2011), however, suggest that North America may have contributed dust to Greenland during the Last Glacial Maximum. Particle size and compositional analyses of GISP2 ice-core dust also suggest that the central United States can act as a dust source during periods of intense drought, such as the Dust Bowl event of the 1930s (Donarummo et al., 2003).

Taken together, these lines of evidence suggest that, while loess-rich areas in Europe and North America cannot be completely ruled out as potential additional dust sources, their overall contribution to the EGRIP S3 ice-core dust is likely limited compared with major source regions in East Asia and North Africa (Figure S7 in Supporting Information S1).

4.2. Changing Contribution of Ice-Core Dust From Potential Sources

Our results suggest that the relative contributions of major dust source regions to the EGRIP site have changed since the mid–late 20th century, characterized by decreasing contributions from Asian sources and increasing contributions from African sources. This interpretation is consistent with previously documented changes in dust emissions and transport patterns over the past several decades.

The mineralogical composition of the EGRIP S3 ice-core dust indicates a shift in dust-source contributions. Although the overall mineral proportion has remained relatively stable over the past century, the relative abundance of specific clay minerals has changed since the 1970s (Figure 3). In particular, the proportion of illite has decreased, while that of high-Si + Al minerals, including kaolinite has increased. In a ternary clay mineralogy diagram, the samples from 1910 to 1970 AD are located in the bottom-right region, close to loess and desert sand from Asia and some loess deposits from North America (Figure 5). In contrast, samples from 1970 to 2013 AD plot toward lower illite/micas/chlorite contents. The difference between pre-and post-1970 samples is statistically significant (permutational multivariate analysis of variance, $p < 0.05$). Previous studies have reported that dust transported from East Asian deserts to Greenland is typically characterized by high illite content, low smectite abundance, and a low kaolinite/chlorite ratio (e.g., Biscaye et al., 1997; Drab et al., 2002; Formenti et al., 2011; Újvári et al., 2022). Újvári et al. (2015) analyzed the clay mineralogy of potential source areas for Greenland ice cores and showed that Chinese loess has a higher illite proportion (64%–71%) than those of Alaskan, central European, and Siberian loess (14%–58%). On the other hand, dust from the western and central Sahara is known to contain abundant kaolinite and have low illite/kaolinite ratios (Scheuvens et al., 2013). The observed decrease in illite and increase in kaolinite in the EGRIP S3 record therefore suggest a reduction in East Asian dust contributions and a greater influence of African dust sources since the 1970s.

A similar shift is also observed in the cluster compositions of quartz particles in the ice-core dust. The cluster compositions (Figure 4) indicate that samples since the 1970s tend to plot closer to the Sahara Desert in North Africa, whereas samples from 1940 to 1950 and 1950–1960 AD plot between the Sahara and Eastern Asian deserts (Gobi and Taklimakan deserts). Although the differences are relatively small, this trend is consistent with the shift suggested by the clay mineral assemblages.

The elemental concentration ratios measured in the ice core further support this interpretation. The concentrations of nssCa (e.g., Drab et al., 2002; Miyamoto et al., 2022; Oyabu et al., 2016; Sinnl et al., 2022; Whitlow et al., 1992), nssK, nssMg, Fe (e.g., Dibb et al., 2007; Kuramoto et al., 2011; Nakazawa et al., 2021), and Al are commonly used as proxies for terrestrial dust in ice cores. In the EGRIP S3 ice core, nssCa accounts for 85%–100% of the total Ca concentration, indicating its primarily continental origin. Scatter plots of nssMg/Al,

21698996, 2026, 22, Downloaded from https://agupubs.onlinelibrary.wiley.com/doi/10.1029/2025JD045800 by NICE, National Institute for Health and Care Excellence, Wiley Online Library on [19/11/2026]. See the Terms and Conditions (https://onlinelibrary.wiley.com/terms-and-conditions) on Wiley Online Library for rules of use; OA articles are governed by the applicable Creative Commons License

Table 2
Summary of Linear Regression Results for Elemental Concentration Ratios of nssMg/Al, nssK/Al, nssCa/Al, and Fe/Al Versus Si/Al by Decade in EGRIP S3 Ice-Core Samples From 1910 to 2013

Decade	nssMg/Al	nssK/Al	nssCa/Al	Fe/Al
1910s	0.0033	**0.1274**	−0.0321	0.0077
1920s	−0.0016	**0.1180**	0.0355	0.0007
1930s	−0.0006	0.0087	−0.0134	0.0090
1940s	−0.0070	**0.0981**	−0.0560	−0.0168
1950s	−0.0006	0.0388	0.0163	0.0132
1960s	**0.0427**	−0.0078	0.0493	**0.0571**
1970s	0.0024	0.0013	0.0041	**0.0147**
1980s	0.0115	0.0223	0.0453	**0.0368**
1990s	−0.0396	0.0661	0.0424	0.0449
2000s	−0.0035	0.0761	0.0531	**0.0687**
2010s	−0.0255	0.0208	−0.1692	−0.1032

Note. Values represent the slopes of linear regression lines. Values in bold indicate statistically significant correlations ($p < 0.05$) with a coefficient of determination (R^2) of ≥0.5; the correlations were calculated using data obtained at intervals of approximately 0.5–1.4 years (See Text S2 in Supporting Information S1, for details of the calculation method).

nssK/Al, nssCa/Al, and Fe/Al concentration ratios versus Si/Al reveal that nssK/Al and Fe/Al show significant correlations with Si/Al (Table 2, Figure S8 in Supporting Information S1). The nssK/Al ratio shows a relatively strong positive correlation with Si/Al from the 1910s to the 1940s (excluding the 1930s), with a weaker positive relationship in the 1950s; however, this correlation weakens after the 1960s. Because nssK is primarily derived from clay illite and potassic feldspar (Formenti et al., 2011) and the EGRIP S3 ice core contains little K-feldspar (Table 1, Figure 3), these results likely reflect a stable contribution of illite-rich Asian dust between the 1910s and 1950s followed by a reduction after the 1960s. In contrast, the correlation between Fe/Al and Si/Al strengthens after the 1960s, with increasing regression slopes, suggesting a growing contribution from Fe-rich dust sources (Table 2). Formenti et al. (2011) reported that mineral dust from the Sahara Desert (PSA NAF-2) has a higher Fe/Al ratio than that of dust from the Gobi Desert (PSA EAS-4). The gradual increase in Fe/Al since the 1960s may therefore reflect an enhanced contribution from African dust sources.

This interpretation based on mineralogical evidence is consistent with previously documented changes in dust emissions and atmospheric circulation over the past several decades. Long-term observations indicate that Saharan dust export increased during the late 20th century, particularly during the prolonged Sahel drought that began in the late 1960s (Nicholson et al., 2000; Prospero & Lamb, 2003; Prospero & Nees, 1986). Previous studies have demonstrated that this increase was associated with large-scale climatic variability, including the Atlantic Multidecadal Oscillation (AMO) and the North Atlantic Oscillation (NAO). During the negative AMO phases, a southward shift of the Intertropical Convergence Zone and cooling of the North Atlantic (e.g., Wang et al., 2012) promote Sahelian droughts and enhance Saharan dust transport to the North Atlantic and Mediterranean regions (e.g., Doherty et al., 2012, 2014). In contrast, meteorological records indicate that East Asian dust activity declined markedly after the late 1970s. The frequency of dust storms decreased to approximately half of the levels observed during the 1950s–1970s (Qian et al., 2002), primarily because of reduced surface wind speeds (e.g., Guan et al., 2017; Liu et al., 2020; Wu et al., 2018). This long-term decline is also supported by independent geological archives, including aeolian dust flux records in sediments from Lake Suigetsu, Japan (Nagashima et al., 2016), and a Tibetan ice core (Huang et al., 2024), which both indicate reduced dust emissions since the mid-20th century.

Additional support for shifts in the contributions from major dust source regions is provided by variations in particle size in the EGRIP S3 ice core. The fine-particle percentage (Figure 6a), which represents the relative abundance of fine particles within the dust size distribution, shows a statistically significant positive correlation with the AMO index after 1950 AD (Table 3, Figure 6b and Figure S9 in Supporting Information S1). Although this relationship alone cannot identify dust sources, it is consistent with the mineralogical evidence indicating an

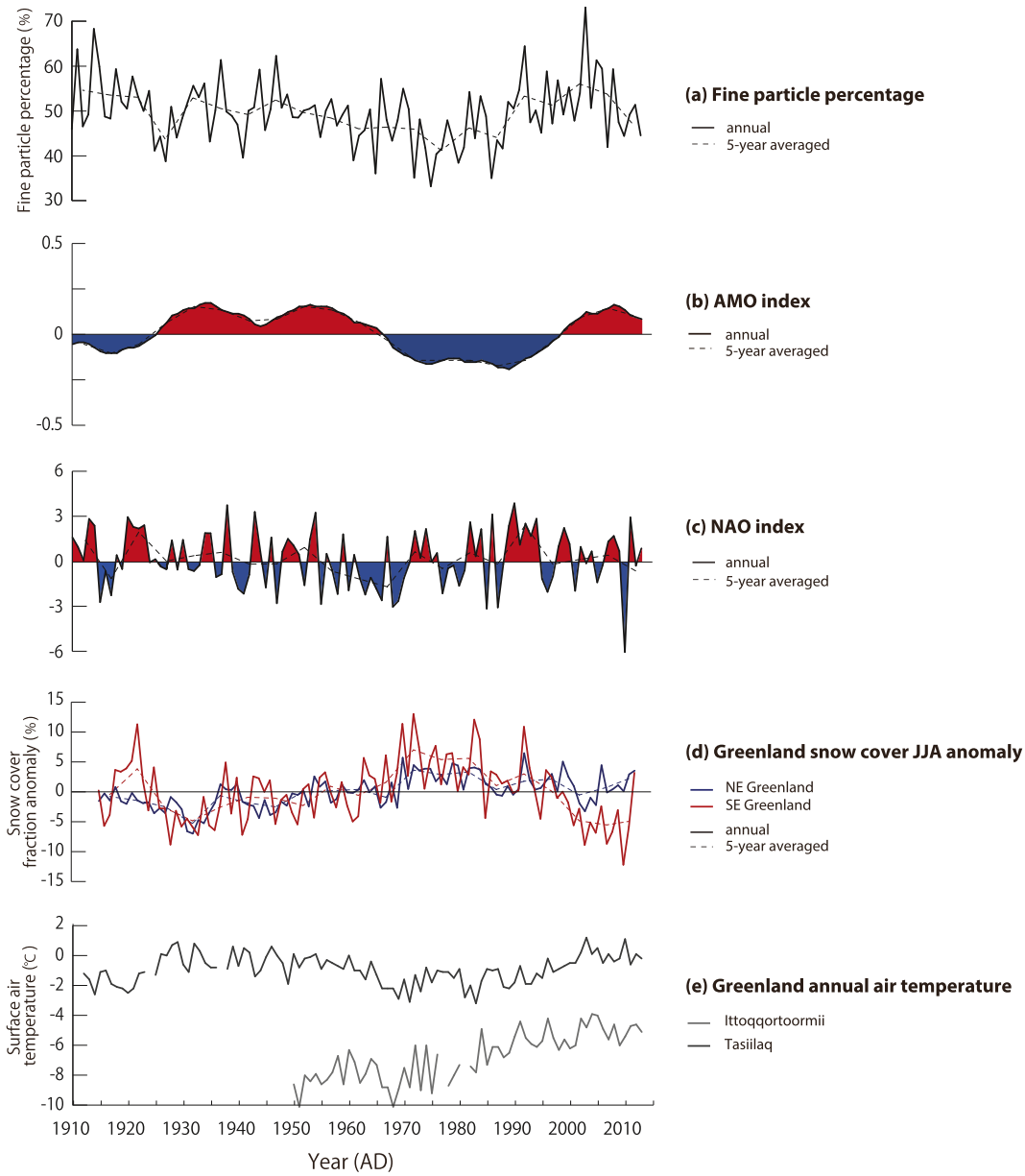


Figure 6. Historical changes in (a) fine-particle percentage of EGRIP S3 ice-core dust particles measured using a Coulter counter. Values represent the ratio of particle number concentration in the fine particle size range (0.70–2.53 μm) to that in the total measured size range (0.70–6.49 μm), following the approach of Delmonte et al. (2004) with particle-size ranges adapted to the measurement limits of the Coulter counter. Data are grouped into ∼0.5–1.3-year intervals; therefore, these are not exact annual averages (see Text S2 in Supporting Information S1, for details of the calculation method). (b) AMO index (Trenberth et al., 2023), (c) NAO index (Hurrell & National Center for Atmospheric Research Staff, 2023), (d) snow cover fraction anomalies, and (e) annual mean surface air temperatures in Greenland. The temperature records for Ittoqqortoormii and Tasiilaq in eastern Greenland, located 750 km southeast and 1100 km south of the EGRIP site, respectively, are from Cappelen (2019). Snow cover fraction anomalies deviate from the 1915–2012 AD average in northeast and southeast Greenland.

increasing contribution of African dust since the 1960s–1970s. Because African dust sources have a shorter transport distance to Greenland than East Asian deserts, an increased contribution of African dust would be expected to result in a relative increase in coarse particles and consequently a decrease in fine-particle percentage. This particle-size interpretation is broadly consistent with the observed positive correlation between fine-particle percentage and the AMO index, given that enhanced Saharan dust transport has been associated with negative

21698996, 2026, 22, Downloaded from https://agupubs.onlinelibrary.wiley.com/doi/10.1029/2025JD045800 by NICE, National Institute for Health and Care Excellence, Wiley Online Library on [19/11/2026]. See the Terms and Conditions (https://onlinelibrary.wiley.com/terms-and-conditions) on Wiley Online Library for rules of use; OA articles are governed by the applicable Creative Commons License

21698996, 2026, 22, Downloaded from https://agupubs.onlinelibrary.wiley.com/doi/10.1029/2025JD045800 by NICE, National Institute for Health and Care Excellence, Wiley Online Library on [19/11/2026]. See the Terms and Conditions (https://onlinelibrary.wiley.com/terms-and-conditions) on Wiley Online Library for rules of use; OA articles are governed by the applicable Creative Commons License

Table 3
Spearman's Rank Correlation Coefficients (ρ) and Corresponding p-Values Between Fine Particle Percentage of EGRIP S3 Ice-Core Dust Particles and AMO and NAO Indices for Three Time Periods (1910–1950, 1950–1980, and 1980–2013)

	AMO index		NAO index	
	ρ	p-value	ρ	p-value
1910–1950	**−0.38**	0.02	0.22	0.18
1950–1980	**0.77**	0.00	0.01	0.94
1980–2013	**0.56**	0.00	0.19	0.29

Note. Values in bold indicate statistically significant correlations ($p < 0.05$).

AMO phases. On the other hand, no significant correlation was found between the NAO index and the fine-particle percentage for any period (Table 3, Figure 6c).

Local dust sources may also contribute to the EGRIP site. Recent warming has reduced snow cover on the east coast of Greenland, likely shortening the duration of snow cover (Figures 6d and 6e) and potentially increasing local dust emissions. Enhanced local dust transport since the 1980s has been reported, particularly along the coastal margins of the Greenland Ice Sheet (Amino et al., 2021; Nagatsuka et al., 2021) and even within the interior ice sheet, including the EGRIP site (Kjær et al., 2022). Analyses of total (soluble + insoluble) concentrations of major elements (Al, Ca, and Fe) and particle size distributions in snow pit samples have revealed seasonal variations in mineral dust sources at the EGRIP site: from winter to spring, most dust originates from distant arid sources, whereas from summer to autumn, a larger proportion comes from Greenland coastal regions (Komuro et al., 2024). These observations suggest that locally derived dust can episodically influence the EGRIP site.

However, several lines of evidence indicate that the relative contribution of local dust to the EGRIP S3 ice-core record analyzed in this study is limited compared to that of long-range transported dust. First, the fine-particle percentage in the EGRIP S3 ice core (Figure 6a) has increased since the 1980s and shows a negative correlation with modeled snow cover fraction anomalies during summer (June–August) on the southeast coast of Greenland (Figure 6d), suggesting that the influence of local dust is likely small. Second, the particle size distribution of the EGRIP S3 dust supports a predominantly distal origin. Simonsen et al. (2019) proposed that particles with diameters smaller than 2 μm and larger than 8 μm in Greenland ice cores can serve as indicators of distant and local sources, respectively. In the EGRIP S3 ice-core samples, particles larger than 8 μm are extremely rare (only 7 particles across all samples), whereas the majority of particles are smaller than 2 μm. Such a fine particle population is consistent with long-range atmospheric transport rather than local emission. Furthermore, the ice-core samples analyzed in this study represent decadal averages. Because locally derived dust at the Greenland Ice Sheet is primarily associated with summer conditions, when dust concentrations at the EGRIP site are relatively low (Komuro et al., 2024), episodic local inputs are likely to be attenuated in the decadal-mean record.

Taken together, these observations suggest that although locally derived dust can reach the EGRIP site, the mineral dust preserved in the EGRIP S3 ice core is largely composed of particles transported over long distances, with local contributions likely representing a secondary component. Under this interpretation, the shift in the primary dust source observed since the 1960s–1970s is most plausibly explained by changes in large-scale dust sources and atmospheric transport patterns, potentially linked to variability in the AMO index and/or a decline in Asian dust events.

4.3. Comparison With Northwestern Greenland Ice-Core Dust (SIGMA-D)

The comparison between the EGRIP S3 and SIGMA-D ice cores reveals two key aspects of mineral dust characteristics: differences in temporal variation trends of silicate mineral composition and differences in overall mineralogical composition, reflecting the degree of local dust contribution and variations among geological source regions, respectively.

21698996, 2026, 22, Downloaded from https://agupubs.onlinelibrary.wiley.com/doi/10.1029/2025JD045800 by NICE, National Institute for Health and Care Excellence, Wiley Online Library on [19/11/2026]. See the Terms and Conditions (https://onlinelibrary.wiley.com/terms-and-conditions) on Wiley Online Library for rules of use; OA articles are governed by the applicable Creative Commons License

The SIGMA-D ice core, drilled near the ice-sheet margin, shows substantial multidecadal variability in silicate mineral composition over the past 100 years, with increases in feldspars (3%–21%), mafic minerals (1%–9%), and quartz (10%–22%) during the warm periods (1915–1949 and 2005–2013 AD), attributed to enhanced inputs from local ice-free areas due to reduced snow/ice cover duration in the coastal region (Nagatsuka et al., 2021; Figure 3). Conversely, the kaolinite group (kaolinite and high-Si + Al minerals, corresponding to Type A in Nagatsuka et al., 2021) constituted a major component of the SIGMA-D dust assemblage and was particularly abundant during the cold periods (1950–2004 AD; 39%–76%). Together with particle-size characteristics and back-trajectory analysis, the high abundance of these minerals was interpreted by Nagatsuka et al. (2021) as reflecting contributions from kaolinite-rich relict deposits in northern Canada. In contrast, the EGRIP S3 ice core, drilled in the interior, exhibits limited temporal variability and generally lower proportions of these minerals (feldspars: 4%–9%, mafic: 0%–4%, quartz: 4%–12%, Table 1), consistent with a minimal influence from local sources. The smaller particle size of EGRIP S3 dust (mean: 0.85–1.36 μm; maximum: 5.06–8.94 μm, Table S2 in Supporting Information S1) compared to that of SIGMA-D dust (mean: 1.02–2.53 μm; maximum: 4.94–26.51 μm, Nagatsuka et al., 2021) further supports a greater influence of long-range transport at the EGRIP site.

These findings align with previous studies that suggested that dust sources depend on the distance of ice-core sites from the ice-sheet margin and/or the altitude of the site (Bory, Biscaye, Piotrowski, & Steffensen, 2003). Specifically, the majority of the dust deposited at interior sites (NGRIP, GRIP, Site-A, and Dye-3) originates from long-range transport from distant deserts, whereas at coastal sites (Hans Tausen and Renland), the primary sources are local ice-free areas.

In addition to the variability, the silicate mineral composition also differs markedly (Figure 3), indicating that the ice-core dust was likely transported from different geological sources. The EGRIP S3 ice core contains much lower proportions of kaolinite-group minerals (10%–26%) and lower proportions of feldspars, mafic minerals, and quartz (considered to be indicators of local dust contributions at the SIGMA-D, as described above), but is enriched in mica/chlorite and illite (21%–37% and 3%–16%, respectively, Table 1, Figure 3) compared to the SIGMA-D ice core (3%–25% and 0%–11%, respectively, Nagatsuka et al., 2021). Thus, the lower kaolinite-group mineral content and feldspar, mafic mineral, and quartz content in the EGRIP S3 ice core may reflect a smaller contribution from northern Canada and coastal Greenland compared to that for the SIGMA-D ice core, respectively. On the other hand, the higher illite content, which is considered to be primarily of Asian origin, as discussed in Section 4.2, is possibly due to a larger contribution from Asian deserts to the EGRIP site. These differences are also reflected in clay mineral assemblages (Figure 5), which primarily represent long-range transported dust and thus support the inferred differences among distal source regions.

Although the back-trajectory analysis has limitations in identifying distant dust sources (Section 4.1), the results provide supplementary information on the differences in the contribution of source regions to ice-core dust between the EGRIP and SIGMA-D sites. To compare transport pathways of mineral dust from the EGRIP S3 ice core with those from the SIGMA-D ice core, we calculated the probability distributions of air masses from 1958 to 2014 AD using the HYSPLIT back-trajectory model. Figures 2b and 2c show the averaged probability distributions for air masses arriving at the EGRIP and SIGMA-D sites, respectively, calculated from 7-day back-trajectories. The pie charts illustrate the cumulative contributions from land regions during these trajectories, calculated according to the regional definitions shown in Figure 2a. There is little interannual variation in the contributions from these source regions. The Greenland coastal regions show the highest overall contributions at both ice-core sites (55%–62%, Figures 2b and 2c), consistent with previous remote-sensing and process-based modeling studies (Groot Zwaaftink et al., 2016; O'Neill et al., 2025), suggesting a strong influence of local and high-latitude dust in the Arctic. However, back-trajectory analysis traces air-mass pathways rather than mineral dust itself, and thus the inferred contributions do not necessarily reflect actual dust-source contributions. In contrast, our mineralogical data indicate that the contribution of locally derived dust to the EGRIP S3 ice core is limited relative to long-range transported dust. Excluding the coastal regions of Greenland, SIGMA-D exhibits a prominent contribution from North America (NA, 93%), whereas EGRIP S3 is characterized by relatively larger contributions from Europe (EU, 20%) and Russia (RUS, 13%). This pattern provides additional context for interpreting the differences in mineral composition observed between the two ice cores.

Our findings identify spatial variations in Greenland ice-core dust characteristics, including size, composition, and sources, between interior and coastal sites and highlight their significance. Ice cores from coastal regions, such as SIGMA-D, contain a larger proportion of locally derived mineral dust, which reflects local environmental

21698996, 2026, 22, Downloaded from https://agupubs.onlinelibrary.wiley.com/doi/10.1029/2025JD045800 by NICE, National Institute for Health and Care Excellence, Wiley Online Library on [19/11/2026]. See the Terms and Conditions (https://onlinelibrary.wiley.com/terms-and-conditions) on Wiley Online Library for rules of use; OA articles are governed by the applicable Creative Commons License

changes, and are therefore important for understanding environmental changes within Greenland. In contrast, ice cores from interior regions, such as EGRIP S3, where local contributions are limited, reflect variations in ground surface and atmospheric conditions in distant dust sources. These interior records are crucial for understanding global environmental changes and provide valuable insights into the dynamics of long-range dust transport to Greenland. The mineralogical characteristics of dust identified in this study may serve as important observational data for future remote sensing and modeling studies.

5. Conclusions

This study presents the first continuous records of morphological and mineralogical properties and provenance of mineral dust in the northeastern Greenland shallow ice core (EGRIP S3) over the past 100 years. These records were obtained through a multi-proxy provenance approach based on individual particle analysis. Our findings highlight the following three key points.

1. The primary sources of the EGRIP S3 ice-core dust are likely East Asian deserts (Gobi [Southern Mongolia] and Taklimakan deserts) and an African desert (Sahara Desert). Certain regions of Europe and North America where loess is abundantly deposited are likely additional sources. These source interpretations are consistent with those identified for other interior Greenland ice-core dust from glacial periods.
2. Our SEM-CL/EDS and elemental concentration results reveal a shift in the relative contribution from the two primary dust sources since the 1960s−1970s, characterized by a decrease in Asian dust and an increase in African dust over the past 50 years. This pattern has not previously been clearly documented in Greenland ice-core mineralogical records. The shift is likely linked to variations in the AMO and the recent decline in Asian dust events.
3. Significant differences in the variability and composition of the EGRIP S3 ice-core dust compared to those of the northwestern coastal Greenland ice core (SIGMA-D) reflect variations in the degree of local dust contribution and geological source regions, respectively. These findings indicate that the sources and transportation processes of mineral dust differ between coastal and interior regions of Greenland. High-temporal-resolution records from interior Greenland sites therefore provide important information on environmental conditions in distant dust source regions that may not be captured in coastal ice cores.

This study demonstrates that even over a relatively short timescale of just 100 years, continuous mineralogical records can reveal shifts in the provenance and composition of ice-core dust, providing important insights into recent changes in atmospheric dust transport and its link with climate variability. However, because the decadal-resolution samples inevitably integrate dust from multiple sources, some degree of mixing cannot be excluded, which introduces uncertainty in deterministic source attribution. Further studies using higher temporal resolution and complementary provenance tracers will therefore be important to better resolve the relative contributions of individual source regions, including those from North America and Europe. In addition, mineralogical reference data from Greenland and other potential Arctic dust source regions remain limited. Expanding these data sets will be important for further evaluating the potential contribution of Arctic dust sources under modern climate conditions, as recently highlighted by modeling studies (e.g., Hopcroft & Rousseau, 2026). Despite these remaining challenges, our findings offer new perspectives on the provenance of Greenland ice-core dust and contribute to paleoenvironmental reconstruction. Moreover, identifying not only the source regions of mineral dust but also its physical and chemical properties (i.e., composition and particle size) and their variability is essential for improving predictions of surface darkening and ice mass loss of the Greenland Ice Sheet, as well as for advancing our understanding of ice-nucleating particles and their influence on atmospheric processes in the Arctic.

Appendix A: Measurements Used for Ice-Core Dating

The chronology of the EGRIP S3 ice core was established based on the sodium (Na), sulfate (SO_4), and tritium concentration profiles (Figure A1). The Na and S concentrations were measured using an inductively coupled plasma mass spectrometry (ICP-MS; 7700, Agilent Technologies, USA) system connected to a continuous-flow analysis (CFA) system at the National Institute of Polar Research (NIPR). Sulfate concentrations were calculated from S concentrations under the assumption that the dominant S-containing species is SO_4. Details of the CFA analysis method are described in Goto-Azuma et al. (2024) and Goto-Azuma et al. (2025).

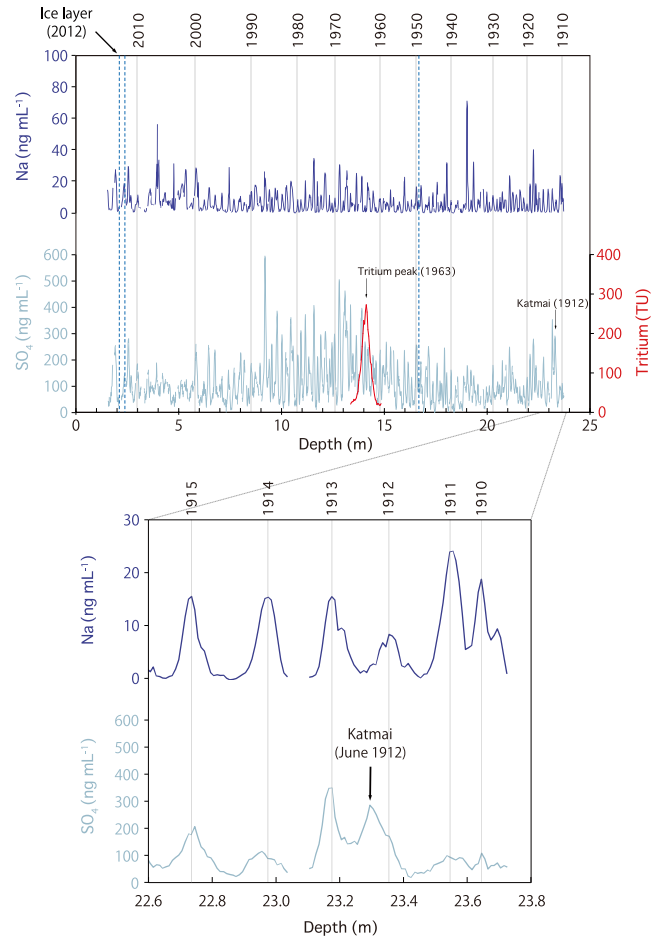


Figure A1. Na, SO_4, tritium, and ice layer (blue dashed line) records in the upper 28.78 m (1880–2013) of the EGRIP S3 ice core (top). Major volcanic signals identified in the SO_4 record are shown. Enlarged view of the 22.6 to 23.725 m (bottom).

The tritium content was measured using a liquid scintillation counting technique at Nagoya University. The ice samples were distilled and mixed with a liquid scintillation cocktail (Ultima Gold LLT, PerkinElmer, USA). Radioactivity associated with tritium was measured using a low-background liquid scintillation counter (Quantulus 1220, PerkinElmer, USA) for 1,500 min. The lower detection limit was about 7 TU and the relative uncertainty was less than 5%.

Conflict of Interest

The authors declare no conflicts of interest relevant to this study.

Availability Statement

The elemental and sulfate concentrations, dust concentrations, and mineralogical and particle-size data used in this study are available at the Arctic Data archive System (ADS) (Nagatsuka et al., 2026; https://doi.org/10.17592/001.2026110201). The tritium concentration data are also available through ADS (Nakazawa et al., 2023; https://doi.org/10.17592/001.2023042501). The AMO index (Trenberth et al., 2023; https://climatedataguide.ucar.edu/climate-data/atlantic-multi-decadal-oscillation-amo) and the NAO index (Hurrell & National Center for Atmospheric Research Staff, 2023; https://climatedataguide.ucar.edu/climate-data/hurrell-north-atlantic-oscillation-nao-index-station-based) were obtained from The University Corporation for Atmospheric Research. ERA5 monthly averaged data on single levels were obtained from the Copernicus Climate Data Store (Hersbach et al., 2020; https://cds.climate.copernicus.eu/). The CMIP6 model output prepared for land-hist, which is a land-

21698996, 2026, 22, Downloaded from https://agupubs.onlinelibrary.wiley.com/doi/10.1029/2025JD045800 by NICE, National Institute for Health and Care Excellence, Wiley Online Library on [19/11/2026]. See the Terms and Conditions (https://onlinelibrary.wiley.com/terms-and-conditions) on Wiley Online Library for rules of use; OA articles are governed by the applicable Creative Commons License

only experiment using climate models with prescribed atmospheric conditions near the land surface using the reanalysis data set GSWP3 (Kim, 2017), is available at the link in the reference list. We used model outputs derived from 12 climate models, namely BCC-CSM2-MR, CESM2, CMCC-ESM2, CNRM-CM6-1, CNRM-ESM2-1, GFDL-ESM4, GISS-E2.1G, HadGEM3-GC31-LL, IPSL-CM6A-LR, MIROC6, MPI-ESM1-2-LR, and UKESM1-0-LL (Boucher et al., 2019; Danabasoglu, 2019; Malyshev et al., 2018; NASA, 2018; Onuma & Kim, 2020; Peano et al., 2020; Stacke et al., 2019; Voldoire, 2019a, 2019b; Wiltshire, 2020; Wiltshire et al., 2020; Zhang et al., 2019).

Acknowledgments

We would like to thank the members of the EGRIP projects for their generous support. EGRIP is directed and organized by the Centre for Ice and Climate at the Niels Bohr Institute, University of Copenhagen. It is supported by funding agencies and institutions in Denmark (A. P. Møller Foundation, University of Copenhagen), USA (US National Science Foundation, Office of Polar Programs), Germany (Alfred Wegener Institute, Helmholtz Centre for Polar and Marine Research), Japan (National Institute of Polar Research and Arctic Challenge for Sustainability), Norway (University of Bergen and Trond Mohn Foundation), Switzerland (Swiss National Science Foundation), France (French Polar Institute Paul-Emile Victor, Institute for Geosciences and Environmental research), Canada (University of Manitoba) and China (Chinese Academy of Sciences and Beijing Normal University). We sincerely appreciate the SEM-CL measurement support provided by Sayuri Kubo. We also would like to thank Hiromi Okumura at NIPR for supporting the Coulter counter analysis. We also thank the two anonymous reviewers, the Associate Editor, and the Editor for their constructive comments and suggestions. This research was supported by the Japan Society for the Promotion of Science KAKENHI (Grants JP18H04140, JP19K20443, JP20K19962, JP22J40168, JP23H00524, JP23K17036, JP26K15148, JP26K15150, and JP26K21780), the Arctic Challenge for Sustainability (ArCS) Project (Grant JPMXD130000000), the Arctic Challenge for Sustainability II (ArCS II) Project (Grant JPMXD1420318865), the Integrated Research Program for Advancing Climate Models (Grant JPMXD0717935457), the Advanced Studies of Climate Change Projection (Grant JPMXD0722680395), and the Environment Research and Technology Development Fund (Grant JPMEERF20172003, JPMEERF20202003, and JPMEERF20232001) of the Environmental Restoration and Conservation Agency of Japan.

References

Alexander, P. M., Tedesco, M., Fettweis, X., van de Wal, R. S. W., Smeets, C. J. P. P., & van den Broeke, M. R. (2014). Assessing spatio-temporal variability and trends in modelled and measured Greenland ice sheet albedo (2000–2013). *The Cryosphere*, *8*(6), 2293–2312. https://doi.org/10.5194/tc-8-2293-2014

Alley, R. B., & Koci, B. R. (1988). Ice-core analysis at site A, Greenland: Preliminary results. *Annals of Glaciology*, *10*, 1–4. https://doi.org/10.3189/S0260305500004067

Amino, T., Iizuka, Y., Matoba, S., Shimada, R., Oshima, N., Suzuki, T., et al. (2021). Increasing dust emission from ice free terrain in southeastern Greenland since 2000. *Polar Science*, *27*, 100599. https://doi.org/10.1016/j.polar.2020.100599

Andersen, K. K., Armengaud, A., & Genthon, C. (1998). Atmospheric dust under glacial and interglacial conditions. *Geophysical Research Letters*, *25*(13), 2281–2284. https://doi.org/10.1029/98GL51811

Atkinson, J. D., Murray, B. J., Woodhouse, M. T., Whale, T. F., Baustian, K. J., Carslaw, K. S., et al. (2013). The importance of feldspar for ice nucleation by mineral dust in mixed-phase clouds. *Nature*, *498*(7454), 355–358. https://doi.org/10.1038/nature12278

Bamber, J. L., Griggs, J. A., Hurkmans, R. T. W. L., Dowdeswell, J. A., Gogineni, S. P., Howat, I., et al. (2013). A new bed elevation dataset for Greenland. *The Cryosphere*, *7*(2), 499–510. https://doi.org/10.5194/tc-7-499-2013

Beer, J., Finkel, R. C., Bonani, G., Gäggeler, H., Görlach, U., Jacob, P., et al. (1991). Seasonal variations in the concentrations of ^{10}Be, Cl^-, NO_3^-, SO_4^{2-}, H_2O_2, ^{210}Pb, ^3H, mineral dust, and $\sigma^{18}O$ in Greenland snow. *Atmospheric Environment, Part A: General Topics*, *25*(5–6), 899–904. https://doi.org/10.1016/0960-1686(91)90131-P

Bigler, M., Wagenbach, D., Fischer, H., Kipfstuhl, J., Miller, H., Sommer, S., & Stauffer, B. (2002). Sulphate record from a northeast Greenland ice core over the last 1200 years based on continuous flow analysis. *Annals of Glaciology*, *35*, 250–256. https://doi.org/10.3189/172756402781817158

Biscaye, P. E., Grousset, F. E., Revel, M., Van der Gaast, S., Zielinski, G. A., Vaars, A., & Kukla, G. (1997). Asian provenance of glacial dust (stage 2) in the Greenland Ice Sheet project 2 ice core, summit, Greenland. *Journal of Geophysical Research: Oceans*, *102*(C12), 26765–26781. https://doi.org/10.1029/97JC01249

Boggs, S., Jr., Kwon, Y.-I., Goles, G. G., Rusk, B. G., Krinsley, D., & Seyedolali, A. (2002). Is quartz cathodoluminescence color a reliable provenance tool? A quantitative examination. *Journal of Sedimentary Research*, *72*(3), 408–415. https://doi.org/10.1306/102501720408

Bory, A. J.-M., Biscaye, P. E., & Grousset, F. E. (2003). Two distinct seasonal Asian source regions for mineral dust deposited in Greenland (NorthGRIP). *Geophysical Research Letters*, *30*(4), 1167. https://doi.org/10.1029/2002GL016446

Bory, A. J.-M., Biscaye, P. E., Piotrowski, A. M., & Steffensen, J. P. (2003). Regional variability of ice core dust composition and provenance in Greenland. *Geochemistry, Geophysics, Geosystems*, *4*(12), 1107. https://doi.org/10.1029/2003GC000627

Boucher, O., Denvil, S., Levavasseur, G., Cozic, A., Caubel, A., Foujols, M. A., et al. (2019). IPSL IPSL-CM6A-LR model output prepared for CMIP6 LS3MIP land-hist. Version 20190321, Earth system grid Federation [Dataset]. *World Data Center for Climate (WDCC)*. https://doi.org/10.22033/ESGF/CMIP6.5205

Buggle, B., Glaser, B., Zöller, L., Hambach, U., Marković, S., Glaser, I., & Gerasimenko, N. (2008). Geochemical characterization and origin of southeastern and eastern European loesses (Serbia, Romania, Ukraine). *Quaternary Science Reviews*, *27*(9–10), 1058–1075. https://doi.org/10.1016/j.quascirev.2008.01.018

Burke, A., Moore, K. A., Sigl, M., Nita, D. C., McConnell, J. R., & Adkins, J. F. (2019). Stratospheric eruptions from tropical and extra-tropical volcanoes constrained using high-resolution sulfur isotopes in ice cores. *Earth and Planetary Science Letters*, *521*, 113–119. https://doi.org/10.1016/j.epsl.2019.06.006

Cappelen, J. (2019). Denmark - DMI historical climate data collection 1768-2018. DMI Report 19-02.

Chandler, D. M., Alcock, J. D., Wadham, J. L., MacKie, S. L., & Telling, J. (2015). Seasonal changes of ice surface characteristics and productivity in the ablation zone of the Greenland Ice Sheet. *The Cryosphere*, *9*(2), 487–504. https://doi.org/10.5194/tc-9-487-2015

Clausen, H. B., & Hammer, C. U. (1988). The Laki and Tambora eruptions as revealed in Greenland ice cores from 11 locations. *Annals of Glaciology*, *10*, 16–22. https://doi.org/10.3189/S0260305500004092

Cook, E., Abbott, P. M., Pearce, N. J. G., Mojtabavi, S., Svensson, A., Bourne, A. J., et al. (2022). Volcanism and the Greenland ice cores: A new tephrochronological framework for the last glacial-interglacial transition (LGIT) based on cryptotephra deposits in three ice cores. *Quaternary Science Reviews*, *292*, 107596. https://doi.org/10.1016/j.quascirev.2022.107596

Cook, J., Edwards, A., Takeuchi, N., & Irvine-Fynn, T. (2016). Cryoconite: The dark biological secret of the cryosphere. *Progress in Physical Geography: Earth and Environment*, *40*(1), 66–111. https://doi.org/10.1177/0309133315616574

Danabasoglu, G. (2019). NCAR CESM2 model output prepared for CMIP6 LS3MIP land-hist. Version 20190128. Earth system grid Federation [Dataset]. *World Data Center for Climate (WDCC)*. https://doi.org/10.22033/ESGF/CMIP6.7650

Deer, F. R. S., Howie, R. A., & Zussman, J. (1993). *An introduction to the rock-forming minerals*. Longman.

Delmonte, B., Petit, J. R., Andersen, K. K., Basile-Doelsch, I., Maggi, V., & Lipenkov, V. Y. (2004). Dust size evidence for opposite regional atmospheric circulation changes over east Antarctica during the last climatic transition. *Climate Dynamics*, *23*(3–4), 427–438. https://doi.org/10.1007/s00382-004-0450-9

DeMott, P. J., & Prenni, A. J. (2010). New directions: Need for defining the numbers and sources of biological aerosols as ice nuclei. *Atmospheric Environment*, *44*(15), 1944–1945. https://doi.org/10.1016/j.atmosenv.2010.02.032

Dibb, J. E., Whitlow, S. I., & Arsenault, M. (2007). Seasonal variations in the soluble ion content of snow at Summit, Greenland: Con- straints from three years of daily surface snow samples. *Atmospheric Environment*, *41*(24), 5007–5019. https://doi.org/10.1016/j.atmosenv.2006.12.010

21698996, 2026, 22, Downloaded from https://agupubs.onlinelibrary.wiley.com/doi/10.1029/2025JD045800 by NICE, National Institute for Health and Care Excellence, Wiley Online Library on [19/11/2026]. See the Terms and Conditions (https://onlinelibrary.wiley.com/terms-and-conditions) on Wiley Online Library for rules of use; OA articles are governed by the applicable Creative Commons License

Doherty, O. M., Riemer, N., & Hameed, S. (2012). Control of Saharan mineral dust transport to Barbados in winter by the intertropical convergence zone over West Africa. *Journal of Geophysical Research*, *117*(19), D19117. https://doi.org/10.1029/2012JD017767

Doherty, O. M., Riemer, N., & Hameed, S. (2014). Role of the convergence zone over West Africa in controlling Saharan mineral dust load and transport in the boreal summer. *Tellus B: Chemical and Physical Meteorology*, *66*(1), 23191. https://doi.org/10.3402/tellusb.v66.23191

Donarummo, J., Ram, M., & Stoermer, E. F. (2003). Possible deposit of soil dust from the 1930's U.S. dust bowl identified in Greenland ice. *Geophysical Research Letters*, *30*(6), 1269. https://doi.org/10.1029/2002GL016641

Drab, E., Gaudichet, A., Jaffrezo, J. L., & Colin, J. (2002). Mineral particles content in recent snow at summit (Greenland). *Atmospheric Environment*, *36*(34), 5365–5367. https://doi.org/10.1016/S1352-2310(02)00470-3

Eyring, V., Bony, S., Meehl, G. A., Senior, C. A., Stevens, B., Stouffer, R. J., & Taylor, K. E. (2016). Overview of the coupled model intercomparison project phase 6 (CMIP6) experimental design and organization. *Geoscientific Model Development*, *9*(5), 1937–1958. https://doi.org/10.5194/gmd-9-1937-2016

Fischer, H., Werner, M., Wagenbach, D., Schwager, M., Thorsteinn- son, T., Wilhelms, F., et al. (1998). Little ice age clearly recorded in northern Greenland ice cores. *Geophysical Research Letters*, *25*(10), 1749–1752. https://doi.org/10.1029/98GL01177

Formenti, P., Schütz, L., Balkanski, Y., Desboeufs, K., Ebert, M., Kandler, K., et al. (2011). Recent progress in understanding physical and chemical properties of African and Asian mineral dust. *Atmospheric Chemistry and Physics*, *11*(16), 8231–8256. https://doi.org/10.5194/acp-11-8231-2011

Fuhrer, K., Wolff, E. W., & Johnsen, S. J. (1999). Timescales for dust variability in the greenland ice core project (GRIP) ice core in the last 100,000 years. *Journal of Geophysical Research*, *104*(D24), 31043–31052. https://doi.org/10.1029/1999JD900929

Gfeller, G., Fischer, H., Bigler, M., Schüpbach, S., Leuenberger, D., & Mini, O. (2014). Representativeness and seasonality of major ion records derived from NEEM firn cores. *The Cryosphere*, *8*(5), 1855–1870. https://doi.org/10.5194/tc-8-1855-2014

Goto-Azuma, K., Dallmayr, R., Ogawa-Tsukagawa, Y., Moteki, N., Mori, T., Ohata, S., et al. (2024). Technical note: High-resolution analyses of concentrations and sizes of refractory black carbon particles deposited in northwestern Greenland over the past 350 years – Part 1: Continuous flow analysis of the SIGMA-D ice core using the wide-range single-particle soot photometer and a high-efficiency nebulizer. *Atmospheric Chemistry and Physics*, *24*(22), 12985–13000. https://doi.org/10.5194/acp-24-12985-2024

Goto-Azuma, K., Homma, T., Saruya, T., Nakazawa, F., Komuro, Y., Nagatsuka, N., et al. (2021). Studies on the variability of the Greenland ice sheet and climate. *Polar Science*, *27*, 100557. https://doi.org/10.1016/j.polar.2020.100557

Goto-Azuma, K., Ogawa-Tsukagawa, Y., Fukuda, K., Fujita, K., Hirabayashi, M., Dallmayr, R., et al. (2025). High-resolution analyses of concentrations and sizes of refractory black carbon particles deposited in northwestern Greenland over the past 350 years – Part 2: Seasonal and temporal trends in refractory black carbon originated from fossil fuel combustion and biomass burning. *Atmospheric Chemistry and Physics*, *25*(1), 657–683. https://doi.org/10.5194/acp-25-657-2025

Götte, T., & Richter, D. K. (2006). Cathodoluminescence characterization of quartz particles in mature arenites. *Sedimentology*, *53*(6), 1347–1359. https://doi.org/10.1111/j.1365-3091.2006.00818.x

Götze, J., Pan, Y., & Müller, A. (2021). Mineralogy and mineral chemistry of quartz: A review. *Mineralogical Magazine*, *85*(5), 639–664. https://doi.org/10.1180/mgm.2021.72

Götze, J., Plötze, M., & Habermann, D. (2001). Origin, spectral characteristics and practical applications of the cathodoluminescence (CL) of quartz – A review. *Mineralogy and Petrology*, *71*(3–4), 225–250. https://doi.org/10.1007/s007100170040

Groot Zwaaftink, C. D., Grythe, H., Skov, H., & Stohl, A. (2016). Substantial contribution of northern high-latitude sources to mineral dust in the Arctic. *Journal of Geophysical Research: Atmospheres*, *121*, 13678–13697. https://doi.org/10.1002/2016JD025482

Guan, Q., Sun, X., Yang, J., Pan, B., Zhao, S., & Wang, L. (2017). Dust storms in Northern China: Long-term spatiotemporal characteristics and climate controls. *Journal of Climate*, *30*(17), 6683–6700. https://doi.org/10.1175/JCLI-D-16-0795.1

Han, C., Hur, S. D., Han, Y., Lee, K., Hong, S., Erhardt, T., et al. (2018). High-resolution isotopic evidence for a potential Saharan provenance of Greenland glacial dust. *Scientific Reports*, *8*(1), 15582. https://doi.org/10.1038/s41598-018-33859-0

Helm, V., Humbert, A., & Miller, H. (2014). Elevation and elevation change of Greenland and Antarctica derived from CryoSat-2. *The Cryosphere*, *8*(4), 1539–1559. https://doi.org/10.5194/tc-8-1539-2014

Hersbach, H., Bell, B., Berrisford, P., Hirahara, S., Horányi, A., Muñoz-Sabater, J., et al. (2020). The ERA5 global reanalysis. *Quarterly Journal of the Royal Meteorological Society*, *146*(730), 1999–2049. https://doi.org/10.1002/qj.3803

Hildreth, W. (1983). The compositionally zoned eruption of 1912 in the Valley of ten thousand smokes, katmai national park, Alaska. *Journal of Volcanology and Geothermal Research*, *18*(1–4), 1–56. https://doi.org/10.1016/0377-0273(83)90003-3

Hildreth, W., & Fierstein, J. (2000). Katmai volcanic cluster and the great eruption of 1912. *GSA Bulletin*, *112*(10), 1594–1620. https://doi.org/10.1130/0016-7606(2000)112<1594:kvcatg>2.0.co;2

Hildreth, W., & Fierstein, J. (2012). *The Novarupta-Katmai eruption of 1912 – Largest eruption of the twentieth century; centennial perspectives*. U.S. Geological Survey Professional Paper.1791

Hodson, A., Cameron, K., Bøggild, C., Irvine-Fynn, T., Langford, H., Pearce, D., & Banwart, S. (2010). The structure, biological activity and biogeochemistry of cryoconite aggregates upon an Arctic valley glacier: Longyearbreen, Svalbard. *Journal of Glaciology*, *56*(196), 349–362. https://doi.org/10.3189/002214310791968403

Hopcroft, P. O., & Rousseau, D. (2026). Model evidence for distinct origins of glacial–interglacial and millennial signals in Greenland dust. *Proceedings of the National Academy of Sciences. U.S.A.*, *123*(14), e2531908123. https://doi.org/10.1073/pnas.2531908123

Huang, J., Li, Y., Fu, C., Chen, F., Fu, Q., Dai, A., et al. (2017). Dryland climate change: Recent progress and challenges. *Review of Geophysics*, *55*(3), 719–778. https://doi.org/10.1002/2016RG000550

Huang, J., Wu, G., Zhao, H., & Xu, B. (2024). Quantifying the contribution of multiple processes to the dust decreasing trend in the Guliya ice core over the past 50 years. *Geophysics Research Letters*, *51*(17), e2024GL110429. https://doi.org/10.1029/2024GL110429

Hurrell, J., & National Center for Atmospheric Research Staff. (2023). The climate data guide: Hurrell north atlantic oscillation (NAO) index (station-based). Retrieved from https://climatedataguide.ucar.edu/climate-data/hurrell-north-atlantic-oscillation-nao-index-station-based

Iizuka, Y., Uemura, R., Fujita, K., Hattori, S., Seki, O., Miyamoto, C., et al. (2018). A 60 year record of atmospheric aerosol depositions preserved in a high-accumulation dome ice core, Southeast Greenland. *Journal of Geophysical Research: Atmospheres*, *123*(1), 574–589. https://doi.org/10.1002/2017JD026733

Jary, Z., & Ciszek, D. (2013). Late Pleistocene loess–palaeosol sequences in Poland and western Ukraine. *Quaternary International*, *296*(16), 37–50. https://doi.org/10.1016/j.quaint.2012.07.009

Joughin, I., Smith, B., Howat, I., Scambos, T., & Moon, T. (2010). Greenland flow variability from ice-sheet-wide velocity mapping. *Journal of Glaciology*, *56*(197), 415–430. https://doi.org/10.3189/002214310792447734

21698996, 2026, 22, Downloaded from https://agupubs.onlinelibrary.wiley.com/doi/10.1029/2025JD045800 by NICE, National Institute for Health and Care Excellence, Wiley Online Library on [19/11/2026]. See the Terms and Conditions (https://onlinelibrary.wiley.com/terms-and-conditions) on Wiley Online Library for rules of use; OA articles are governed by the applicable Creative Commons License

Keegan, K. M., Albert, M. R., McConnell, J. R., & Baker, I. (2014). Climate change and forest fires synergistically drive widespread melt events of the Greenland Ice Sheet. *Proceedings of the National Academy of Sciences of the United States of America*, *111*(22), 7964–7967. https://doi.org/10.1073/pnas.1405397111

Kim, H. (2017). Global soil wetness project phase 3 atmospheric boundary conditions (experiment 1) [Dataset]. *Data Integration and Analysis System (DIAS)*. https://doi.org/10.20783/DIAS.501

Kjær, H. A., Vallelonga, P., Svensson, A., Elleskov, L., Kristensen, M., Tibuleac, C., & Kipfstuhl, S. (2016). An optical dye method for continuous determination of Acidity in ice cores. *Environmental Science and Technology*, *50*(19), 10485–10493. https://doi.org/10.1021/acs.est.6b00026

Kjær, H. A., Zens, P., Black, S., Lund, K. H., Svensson, A., & Vallelonga, P. (2022). Canadian forest fires, Icelandic volcanoes and increased local dust observed in six shallow Greenland firn cores. *Climate of the Past*, *18*(10), 2211–2230. https://doi.org/10.5194/cp-18-2211-2022

Koide, M., Michel, R., Goldberg, E., Herron, M. M., & Langway, C. C. (1982). Characterization of radioactive fallout from pre- and post-moratorium tests to polar ice caps. *Nature*, *296*(5857), 544–547. https://doi.org/10.1038/296544a0

Komuro, Y., Nakazawa, F., Goto-Azuma, K., Hirabayashi, M., Shigeyama, W., Koji, F., et al. (2024). Major metallic elements (Al, Ca, and Fe) and size distribution of mineral particles in recent snow in inland northeast Greenland. *Bulletin of Glaciological Research*, *42*, 49–60. https://doi.org/10.5331/bgr.24A02

Komuro, Y., Nakazawa, F., Hirabayashi, M., Goto-Azuma, K., Nagatsuka, N., Shigeyama, W., et al. (2021). Temporal and spatial variabilities in surface mass balance at the EGRIP site, Greenland from 2009 to 2017. *Polar Science*, *27*, 100568. https://doi.org/10.1016/j.polar.2020.100568

Kuramoto, T., Goto-Azuma, K., Hirabayashi, M., Miyake, T., Motoyama, H., Dahl-Jensen, D., & Steffensen, J. P. (2011). Seasonal variations of snow chemistry at NEEM, Greenland. *Annals of Glaciology*, *52*(58), 193–200. https://doi.org/10.3189/172756411797252365

Kurosaki, Y., Matoba, S., Iizuka, Y., Niwano, M., Tanikawa, T., Ando, T., et al. (2020). Reconstruction of sea ice concentration in northern Baffin Bay using deuterium excess in a coastal ice core from the northwestern Greenland Ice Sheet. *Journal of Geophysical Research: Atmospheres*, *125*(16), e2019JD031668. https://doi.org/10.1029/2019JD031668

Legrand, M., & Mayewski, P. (1997). Glaciochemistry of polar ice cores: A review. *Reviews of Geophysics*, *35*(3), 219–243. https://doi.org/10.1029/96RG03527

Liu, J., Wu, D., Liu, G., Mao, R., Chen, S., Ji, M., et al. (2020). Impact of Arctic amplification on declining spring dust events in East Asia. *Climate Dynamics*, *54*(3–4), 1913–1935. https://doi.org/10.1007/s00382-019-05094-4

Lupker, M., Aciego, S. M., Bourdon, B., Schwander, J., & Stocker, T. F. (2010). Isotopic tracing (Sr, Nd, U and Hf) of continental and marine aerosols in an 18th century section of the Dye-3 ice core (Greenland). *Earth and Planetary Science Letters*, *295*(1–2), 277–286. https://doi.org/10.1016/j.epsl.2010.04.010

Maggi, V. (1997). Mineralogy of atmospheric microparticles deposited along the Greenland Ice core project ice core. *Journal of Geophysical Research: Oceans*, *102*(C12), 26725–26734. https://doi.org/10.1029/97JC00613

Mahowald, N., Albani, S., Engelstaedter, S., Winckler, G., & Goman, M. (2011). Model insight into glacial–interglacial paleodust records. *Quaternary Science Reviews*, *30*(7–8), 832–854. https://doi.org/10.1016/j.quascirev.2010.09.007

Malyshev, S., Blanton, C., McHugh, C., Rand, K., Nikonov, S., Radhakrishnan, A., et al. (2018). GFDL-ESM4 model output prepared for CMIP6 LUMIP land-hist, version 20180701, Earth system grid Federation [Dataset]. *World Data Center for Climate (WDCC)*. https://doi.org/10.22033/ESGF/CMIP6.8611

Meese, D. A., Gow, A. J., Grootes, P., Stuiver, M., Mayewski, P. A., Zielinski, G. A., et al. (1994). The accumulation record from the GISP2 core as an indicator of climate change throughout the Holocene. *Science*, *266*(5191), 1680–1682. https://doi.org/10.1126/science.266.5191.1680

Miyamoto, C., Iizuka, Y., Matoba, S., Hattori, S., & Takahashi, Y. (2022). Gypsum formation from calcite in the atmosphere recorded in aerosol particles transported and trapped in Greenland ice core sample is a signature of secular change of SO2 emission in east Asia. *Atmospheric Environment*, *278*(1), 119061. https://doi.org/10.1016/j.atmosenv.2022.119061

Muhs, D. R., Bettis III, E. A., Been, J., & McGeehin, J. P. (2001). Impact of climate and parent material on chemical weathering in loess-derived soils of the Mississippi River valley. *Soil Science Society of America Journal*, *65*, 1761–1777. https://doi.org/10.2136/sssaj2001.1761

Murray, B. J., O'Sullivan, D., Atkinson, J. D., & Webb, M. E. (2012). Ice nucleation by particles immersed in supercooled cloud droplets. *Chemical Society Reviews*, *41*(19), 6519–6554. https://doi.org/10.1039/c2cs35200a

Nagashima, K., Goto-Azuma, K., Ito, A., Hirabayashi, M., Shiraiwa, T., Matoba, S., et al. (2026). Trans-Pacific Saharan dust recorded in Mount Logan ice core. *Progress in Earth and Planetary Science*, *13*(1), 12. https://doi.org/10.1186/s40645-026-00796-w

Nagashima, K., Kawakami, H., Sugie, K., Fujiki, T., Nishioka, J., Iwamoto, Y., et al. (2023). Asian dust-deposition flux to the subarctic Pacific estimated using single quartz particles. *Scientific Reports*, *13*(1), 15424. https://doi.org/10.1038/s41598-023-41201-6

Nagashima, K., Nishido, H., Kayama, M., Kurosaki, Y., Ohgo, S., & Hasegawa, H. (2017). Composition of Asian dust from cathodoluminescence spectral analysis of single quartz grains. *Geology*, *45*, 879–882. https://doi.org/10.1130/G39237.1

Nagashima, K., Suzuki, Y., Irino, T., Nakagawa, T., Tada, R., Hara, Y., et al. (2016). Asian dust transport during the last century recorded in Lake Suigetsu sediments. *Geophysical Research Letters*, *43*(6), 2835–2842. https://doi.org/10.1002/2015GL067589

Nagatsuka, N., Goto-Azuma, K., Nagashima, K., Fujita, K., Komuro, Y., Hirabayashi, M., et al. (2026). A 100-year record of elemental concentrations, dust particle size, and mineralogical composition from a northeastern Greenland shallow ice core (EGRIP S3) (Version 1.00) [Dataset]. *Arctic and Antarctic Data archive System (ADS), Japan*. https://doi.org/10.17592/001.2026110201

Nagatsuka, N., Goto-Azuma, K., Tsushima, A., Fujita, K., Matoba, S., Onuma, Y., et al. (2021). Variations in mineralogy of dust in an ice core obtained from northwestern Greenland over the past 100 years. *Climate of the Past*, *17*(3), 1341–1362. https://doi.org/10.5194/cp-17-1341-2021

Nagatsuka, N., Takeuchi, N., Shin, K. C., & Nakano, T. (2018). Spatial variations of Sr–Nd isotopic ratios, mineralogical and elemental compositions of cryoconite in an Alaskan glacier. *Annals of Glaciology*, *59*(77), 147–158. https://doi.org/10.1017/aog.2019.2

Nagatsuka, N., Takeuchi, N., Uetake, J., Shimada, R., Onuma, Y., Tanaka, S., & Nakano, T. (2016). Variations in Sr and Nd isotopic ratios of mineral particles in cryoconite in Western Greenland. *Frontiers in Earth Science*, *4*, 93. https://doi.org/10.3389/feart.2016.00093

Nakazawa, F., Goto-Azuma, K., Komuro, Y., & Kurita, N. (2023). Tritium data of EGRIP S3 ice core, 1.00 [Dataset]. *Arctic and Antarctic Data archive System (ADS), Japan*. https://doi.org/10.17592/001.2023042501

Nakazawa, F., Nagatsuka, N., Hirabayashi, M., Goto-Azuma, K., Steffensen, J. P., & Dahl-Jensen, D. (2021). Variation in recent annual snow deposition and seasonality of snow chemistry at the east Greenland ice core project (EGRIP) camp, Greenland. *Polar Science*, *27*, 100597. https://doi.org/10.1016/j.polar.2020.100597

NASA Goddard Institute for Space Studies (NASA/GISS). (2018). NASA-GISS GISS-E2.1G model output prepared for CMIP6 LUMIP land-hist, version 20181020, Earth system grid Federation [Dataset]. *World Data Center for Climate (WDCC)*. https://doi.org/10.22033/ESGF/CMIP6.7179

21698996, 2026, 22, Downloaded from https://agupubs.onlinelibrary.wiley.com/doi/10.1029/2025JD045800 by NICE, National Institute for Health and Care Excellence, Wiley Online Library on [19/11/2026]. See the Terms and Conditions (https://onlinelibrary.wiley.com/terms-and-conditions) on Wiley Online Library for rules of use; OA articles are governed by the applicable Creative Commons License

Nicholson, S. E., Some, B., & Kone, B. (2000). An Analysis of Recent Rainfall Conditions in West Africa, Including the Rainy Seasons of the 1997 El Niño and the 1998 La Niña Years. *Journal of Climate*, *13*(14), 2628–2640. https://doi.org/10.1175/1520-0442(2000)013<2628:AAORRC>2.0.CO;2

O'Neill, N. T., Ranjbar, K., Ivănescu, L., Blanchard, Y., Sayedain, S. A., & AboEl-Fetouh, Y. (2025). Remote-sensing detectability of airborne Arctic dust. *Atmospheric Chemistry and Physics*, *25*, 27–44. https://doi.org/10.5194/acp-25-27-2025

Onuma, Y., & Kim, H. (2020). MIROC6 model output prepared for CMIP6 LS3MIP land-hist, version 20200423, Earth system grid Federation [Dataset]. *World Data Center for Climate (WDCC)*. https://doi.org/10.22033/ESGF/CMIP6.5622

Oyabu, I., Matoba, S., Yamasaki, T., Kadota, M., & Iizuka, Y. (2016). Seasonal variations in the major chemical species of snow at the South East Dome in Greenland. *Polar Science*, *10*(1), 36–42. https://doi.org/10.1016/j.polar.2016.01.003

Parvin, F., Seki, O., Fujita, K., Iizuka, Y., Matoba, S., Ando, T., & Sawada, K. (2019). Assessment for paleoclimatic utility of biomass burning tracers in SE-Dome ice core, Greenland. *Atmospheric Environment*, *196*, 86–94. https://doi.org/10.1016/j.atmosenv.2018.10.012

Peano, D., Lovato, T., & Materia, S. (2020). CMCC-ESM2 model output prepared for CMIP6 LS3MIP land-hist, version 20200225, Earth system grid Federation [Dataset]. *World Data Center for Climate (WDCC)*. https://doi.org/10.22033/ESGF/CMIP6.13204

Prospero, J. M., & Lamb, P. J. (2003). African droughts and dust transport to the Caribbean: Climate change implications. *Science*, *302*(5647), 1024–1027. https://doi.org/10.1126/science.1089915

Prospero, J. M., & Nees, R. (1986). Impact of the North African drought and El Niño on mineral dust in the Barbados trade winds. *Nature*, *320*, 735–738. https://doi.org/10.1038/320735a0

Qian, W., Quan, L., & Shi, S. (2002). Variations of the dust storm in China and its climatic control. *Journal of Climate*, *15*(10), 1216–1229. https://doi.org/10.1175/1520-0442(2002)015<1216:votdsi>2.0.co;2

Ruth, U., Wagenbach, D., Steffensen, J. P., & Bigler, M. (2003). Continuous record of microparticle concentration and size distribution in the central Greenland NGRIP ice core during the last glacial period. *Journal of Geophysical Research*, *108*, 4098. https://doi.org/10.1029/2002jd002376

Savarino, J., & Legrand, M. (1998). High northern latitude forest fires and vegetation emissions over the last millennium inferred from the chemistry of a central Greenland ice core. *Journal of Geophysical Research*, *103*(D7), 8267–8279. https://doi.org/10.1029/97JD03748

Scheuvens, D., Schütz, L., Kandler, K., Ebert, M., & Weinbruch, S. (2013). Bulk composition of northern African dust and its source sediments – A compilation. *Earth-Science Reviews*, *116*, 170–194. https://doi.org/10.1016/j.earscirev.2012.08.005

Schüpbach, S., Fischer, H., Bigler, M., Erhardt, T., Gfeller, G., Leuenberger, D., et al. (2018). Greenland records of aerosol source and atmospheric lifetime changes from the eemian to the Holocene. *Nature Communications*, *9*(1), 1476. https://doi.org/10.1038/s41467-018-03924-3

Severin, K. P. (2004). *Energy dispersive spectrometry of common rock forming minerals*. Kluwer Academic Publishers.

Shimada, R., Takeuchi, N., & Aoki, T. (2016). Inter-annual and geographical variations in the extent of bare ice and dark ice on the Greenland Ice Sheet derived from MODIS satellite images. *Frontiers in Earth Science*, *4*, 43. https://doi.org/10.3389/feart.2016.00043

Simonsen, M. F., Baccolo, G., Blunier, T., Borunda, A., Delmonte, B., Frei, R., et al. (2019). East Greenland ice core dust record reveals timing of Greenland ice sheet advance and retreat. *Nature Communications*, *10*(1), 4494. https://doi.org/10.1038/s41467-019-12546-2

Singer, A., Dultz, S., & Argamann, E. (2004). Properties of the non-soluble fractions of suspended dust over the Dead Sea. *Atmospheric Environment*, *38*(12), 1745–1753. https://doi.org/10.1016/j.atmosenv.2003.12.026

Sinnl, G., Winstrup, M., Erhardt, T., Cook, E., Jensen, C. M., Svensson, A., et al. (2022). A multi-ice-core, annual-layer-counted Greenland ice-core chronology for the last 3800 years: GICC21. *Climate of the Past*, *18*(5), 1125–1150. https://doi.org/10.5194/cp-18-1125-2022

Stacke, T., Wieners, K., Giorgetta, M., Jungclaus, J., Reick, C., Esch, M., et al. (2019). MPI-ESM1.2-LR model output prepared for CMIP6 LS3MIP land-hist, version 20190815, Earth system grid Federation [Dataset]. *World Data Center for Climate (WDCC)*. https://doi.org/10.22033/ESGF/CMIP6.6620

Steffensen, J. (1997). The size distribution of microparticles from selected segments of the Greenland Ice core project ice core representing different climatic periods. *Journal of Geophysical Research: Oceans*, *102*(C12), 26755–26763. https://doi.org/10.1029/97JC01490

Stein, A. F., Draxler, R. R., Rolph, G. D., Stunder, B. J. B., Cohen, M. D., & Ngan, F. (2015). NOAA's HYSPLIT atmospheric transport and dispersion modeling system. *Bulletin of the American Meteorological Society*, *96*(12), 2059–2077. https://doi.org/10.1175/BAMS-D-14-00110.1

Svensson, A., Biscaye, P. E., & Grousset, F. E. (2000). Characterization of late glacial continental dust in the Greenland ice core project ice core. *Journal of Geophysical Research*, *105*(D4), 4637–4656. https://doi.org/10.1029/1999JD901093

Takeuchi, N., Nagatsuka, N., Uetake, J., & Shimada, R. (2014). Spatial variations in impurities (cryoconite) on glaciers in northwest Greenland. *Bulletin of Glaciological Research*, *32*, 85–94. https://doi.org/10.5331/bgr.32.85

Trenberth, K., & Zhang, R., & National Center for Atmospheric Research Staff. (2023). The climate data guide: Atlantic Multi-decadal oscillation (AMO). Retrieved from https://climatedataguide.ucar.edu/climate-data/atlantic-multi-decadal-oscillation-amo

Újvári, G., Klötzli, U., Stevens, T., Svensson, A., Ludwig, P., Vennemann, T., et al. (2022). Greenland ice core record of last glacial dust sources and atmospheric circulation. *Journal of Geophysical Research: Atmospheres*, *127*(15), e2022JD036597. https://doi.org/10.1029/2022JD036597

Újvári, G., Stevens, T., Svensson, A., Klotzli, U. S., Manning, C., Németh, T., et al. (2015). Two possible source regions for central Greenland last glacial dust. *Geophysical Research Letters*, *42*(23), 10399–10408. https://doi.org/10.1002/2015GL066153

Vallelonga, P., Christianson, K., Alley, R. B., Anandakrishnan, S., Christian, J. E. M., Dahl-Jensen, D., et al. (2014). Initial results from geophysical surveys and shallow coring of the Northeast Greenland Ice Stream (NEGIS). *The Cryosphere*, *8*(4), 1275–1287. https://doi.org/10.5194/tc-8-1275-2014

Vallelonga, P., & Svensson, A. (2014). In P. Knippertz & J.-B. Stuut (Eds.), *Mineral dust - A key player in the Earth system* (Vol. 18, pp. 463–486). Springer.

van den Hurk, B., Kim, H., Krinner, G., Seneviratne, S. I., Derksen, C., Oki, T., et al. (2016). LS3MIP (v1.0) contribution to CMIP6: The land Surface, snow and soil moisture model intercomparison project – Aims, setup and expected outcome. *Geoscientific Model Development*, *9*(8), 2809–2832. https://doi.org/10.5194/gmd-9-2809-2016

Voldoire, A. (2019a). CNRM-CM6-1 model output prepared for CMIP6 LS3MIP land-hist, version 20191107, Earth system grid Federation [Dataset]. *World Data Center for Climate (WDCC)*. https://doi.org/10.22033/ESGF/CMIP6.4095

Voldoire, A. (2019b). CNRM-ESM2-1 model output prepared for CMIP6 LS3MIP land-hist, version 20190820, Earth system grid Federation [Dataset]. *World Data Center for Climate (WDCC)*. https://doi.org/10.22033/ESGF/CMIP6.9599

Volz, F. E. (1975a). Distribution of turbidity after the 1912 Katmai eruption in Alaska. *Journal of Geophysical Research*, *80*(18), 2643–2648. https://doi.org/10.1029/jc080i018p02643

Volz, F. E. (1975b). Burden of volcanic dust and nuclear debris after injection into the stratosphere at 40°–58°N. *Journal of Geophysical Research*, *80*(18), 2649–2652. https://doi.org/10.1029/JC080i018p02649

21698996, 2026, 22, Downloaded from https://agupubs.onlinelibrary.wiley.com/doi/10.1029/2025JD045800 by NICE, National Institute for Health and Care Excellence, Wiley Online Library on [19/11/2026]. See the Terms and Conditions (https://onlinelibrary.wiley.com/terms-and-conditions) on Wiley Online Library for rules of use; OA articles are governed by the applicable Creative Commons License

Wang, C., Dong, S., Evan, A. T., Foltz, G. R., & Lee, S. K. (2012). Multidecadal covariability of North Atlantic sea surface temperature, African dust, Sahel rainfall, and Atlantic hurricanes. *Journal of Climate*, *25*(15), 5404–5415. https://doi.org/10.1175/JCLI-D-11-00413.1

Webb, N. P., & Pierre, C. (2018). Quantifying anthropogenic dust emissions. *Earth's Future*, *6*(2), 286–295. https://doi.org/10.1002/2017EF000766

Whitlow, S., Mayewski, P. A., & Dibb, J. E. (1992). A comparison of major chemical species seasonal concentration and accumulation at the South Pole and summit, Greenland. *Atmospheric Environment, Part A: General Topics*, *26*(11), 2045–2054. https://doi.org/10.1016/0960-1686(92)90089-4

Wientjes, I. G. M., Van de Wal, R. S. W., Reichart, G. J., Sluijs, A., & Oerlemans, J. (2011). Dust from the dark region in the western ablation zone of the Greenland Ice Sheet. *The Cryosphere*, *5*(3), 589–601. https://doi.org/10.5194/tc-5-589-2011

Wiltshire, A. (2020). UKESM1.0-LL model output prepared for CMIP6 LUMIP land-hist, version 20200806, Earth system grid Federation [Dataset]. *World Data Center for Climate (WDCC)*. https://doi.org/10.22033/ESGF/CMIP6.6143

Wiltshire, A., Liddicoat, S., & Robertson, E. (2020). HadGEM3-GC31-LL model output prepared for CMIP6 LUMIP land-hist, version 20200807, Earth system grid Federation [Dataset]. *World Data Center for Climate (WDCC)*. https://doi.org/10.22033/ESGF/CMIP6.14496

Wu, C., Lin, Z., Liu, X., Li, Y., Lu, Z., & Wu, M. (2018). Can climate models reproduce the decadal change of dust aerosol in East Asia? *Geophysical Research Letters*, *45*(18), 9953–9962. https://doi.org/10.1029/2018GL079376

Wu, G., Zhang, X., Zhang, C., & Xu, T. (2016). Mineralogical and morphological properties of individual dust particles in ice cores from the Tibetan Plateau. *Journal of Glaciology*, *62*(231), 46–53. https://doi.org/10.1017/jog.2016.8

Yalcin, K., Wake, C. P., Kreutz, K. J., Germani, M. S., & Whitlow, S. I. (2007). Ice core paleovolcanic records from the st. Elias Mountains, Yukon, Canada. *Journal of Geophysical Research Atmosphere*, *112*(D8), D08102. https://doi.org/10.1029/2006JD007497

Zhang, Y., Wu, T., Shi, X., Zhang, F., Li, J., Chu, M., et al. (2019). BCC-CSM2MR model output prepared for CMIP6 LUMIP land-hist, version 20190731, Earth system grid Federation [Dataset]. *World Data Center for Climate (WDCC)*. https://doi.org/10.22033/ESGF/CMIP6.2961

Zinkernagel, U. (1978). *Cathodoluminescence of quartz and its application to sandstone petrology, contributions to sedimentology* (Vol. 8). Schweizerbart Science Publishers

References From the Supporting Information

Chester, R., Elderfield, H., Griffin, J. J., Johnson, L. R., & Padgham, C. (1972). Eolian dust along the eastern margins of the Atlantic Ocean. *Marine Geology*, *13*(2), 91–105. https://doi.org/10.1016/0025-3227(72)90048-5

Martinez-Lamas, R., Toucanne, S., Debret, M., Riboulot, V., Deloffre, J., Boissier, A., et al. (2020). Linking danube river activity to alpine ice-sheet fluctuations during the last glacial (ca. 33–17 ka BP): Insights into the continental signature of Heinrich Stadials. *Quaternary Science Reviews*, *229*(1), 106136. https://doi.org/10.1016/j.quascirev.2019.106136

Potter, P. E., Heling, D., Shimp, N. E., & van Wie, W. (1975). Clay mineralogy of modern alluvial muds of the Mississippi River Basin. *Bulletin du Centre Recherche Pau*, *2*, 353–389.

Ro, S., Park, J., Yoo, H., Han, C., Lee, A., Kim, M., et al. (2024). Millennial-scale variability of Greenland dust provenance during the last glacial maximum as determined by single particle analysis. *Scientific Reports*, *14*(1), 2040. https://doi.org/10.1038/s41598-024-52546-x

Sionneau, T., Bout-Roumazeilles, V., Biscaye, P. E., Van VlietLanoe, B., & Bory, A. (2008). Clay mineral distributions in and around the Mississippi River watershed and Northern Gulf of Mexico: Sources and transport patterns. *Quaternary Science Reviews*, *27*(17–18), 1740–1751. https://doi.org/10.1016/j.quascirev.2008.07.001

Skonieczny, C., Bory, A., Bout-Roumazeilles, V., Abouchami, W., Galer, S. J. G., Crosta, X., et al. (2011). The 7-13 March 2006 major Saharan outbreak: Multiproxy characterization of mineral dust deposited on the West African margin. *Journal of Geophysical Research*, *116*(D18), D18210. https://doi.org/10.1029/2011JD016173

Stevens-Kalceff, M. A. (2009). Cathodoluminescence microcharacterization of point defects in α-quartz. *Mineralogical Magazine*, *73*(4), 585–605. https://doi.org/10.1180/minmag.2009.073.4.585

Windom, H. L. (1969). Atmospheric dust records in permanent snowfields: Implications to marine sedimentation. *GSA Bulletin*, *80*(5), 761–782. https://doi.org/10.1130/0016-7606(1969)80[761:adrips]2.0.co;2

21698996, 2026, 22, Downloaded from https://agupubs.onlinelibrary.wiley.com/doi/10.1029/2025JD045800 by NICE, National Institute for Health and Care Excellence, Wiley Online Library on [19/11/2026]. See the Terms and Conditions (https://onlinelibrary.wiley.com/terms-and-conditions) on Wiley Online Library for rules of use; OA articles are governed by the applicable Creative Commons License